batteries

Review

Synergistic Heteroatom Doping in Hard Carbon Anodes: Unlocking High Performance in Potassium-Ion Batteries

Narasimharao Kitchamsetti [1,*], Sungwook Mhin [2,*], HyukSu Han [3,*] and Ana L. F. de Barros [4,*]

[1] Department of Microsystems, University of South-Eastern Norway, Campus Vestfold, Raveien 215, 3184 Borre, Norway
[2] Department of Energy and Materials Engineering, Dongguk University, Seoul 04620, Republic of Korea
[3] Division of Materials Science and Engineering, Hanyang University, Seoul 04763, Republic of Korea
[4] Laboratory of Experimental and Applied Physics, Centro Federal de Educação Tecnológica Celso Suckow da Fonseca, Av. Maracanã Campus 229, Rio de Janeiro 20271-110, Brazil
* Correspondence: narasimharao.kitchamsetti@usn.no (N.K.); swmhin@dongguk.edu (S.M.); hyuksuhan@hanyang.ac.kr (H.H.); ana.barros@cefet-rj.br (A.L.F.d.B.)

Abstract

The increasing demand for energy storage systems that deliver both high performance and environmental sustainability has driven significant interest in potassium-ion batteries (PIBs) as viable substitutes for lithium-ion batteries (LIBs). However, their large-scale application remains constrained by inherent drawbacks, such as limited energy density, poor cycling stability, and suboptimal electrochemical performance. Among various anode candidates, hard carbon (HC) has attracted considerable attention owing to its structural robustness and large specific surface area (SSA). Recent research indicates that heteroatom doping is an effective strategy to enhance the electrochemical properties of HC, leading to improved potassium (K) storage capacity, superior rate performance, and extended cycle life. This review summarizes recent progress in doped HC anodes, with a particular focus on the transition from single-element doping to multi-element doping approaches. The synergistic interactions within multi-dopant systems are systematically discussed, highlighting their potential to overcome the shortcomings of single-doped materials and achieve comprehensive performance improvements. Finally, current challenges and future perspectives for the development of advanced doped HC anodes in PIBs are outlined.

Keywords: hard carbon; multi-heteroatom doping; synergistic effect; potassium-ion batteries; electrochemical properties

1. Introduction

The escalating global energy demand, coupled with the rapid growth of portable electronic devices and electric vehicles (EVs), has intensified the need for energy storage systems that combine high performance with economic and environmental sustainability [1,2]. Conventional technologies, particularly lithium-ion batteries (LIBs), are increasingly challenged by the scarcity of lithium resources and rising manufacturing costs, prompting the exploration of alternative battery chemistries. Among these, potassium-ion batteries (PIBs) have emerged as promising candidates [3–5]. Their advantages stem from the use of potassium ions (K^+) as charge carriers [6–8]. Compared with Li, K is more abundant and more uniformly distributed across the globe, which supports resource sustainability and lowers material costs [9]. Additionally, the affordability of K-based materials

Check for updates

Received: 18 March 2026
Revised: 7 April 2026
Accepted: 9 April 2026
Published: 14 April 2026

Copyright: © 2026 by the authors. Licensee MDPI, Basel, Switzerland. This article is an open access article distributed under the terms and conditions of the Creative Commons Attribution (CC BY) license.

makes PIBs highly suitable for large-scale applications, including grid energy storage and electric transportation.

Carbonaceous materials, including graphite [10], soft carbon (C) [11], and hard C (HC) [12], have been extensively explored as anode candidates for alkali-ion batteries. Graphite, a well-established anode material in LIBs, exhibits limited suitability for K^+ storage due to its small interlayer spacing and poor structural stability upon accommodating large K^+ ions [10]. Soft C, characterized by partially ordered graphitic domains, offers improved electrical conductivity and structural flexibility; however, its relatively limited interlayer spacing and moderate capacity restrict its performance in PIB systems [11]. In contrast, HC, with its highly disordered structure, enlarged interlayer spacing, and abundant microporosity, provides sufficient active sites and buffering capability for K^+ storage, making it a more favorable anode material for PIBs [12].

HC is widely regarded as a highly promising anode material for PIBs owing to its excellent structural stability, large specific surface area (SSA), and favorable K^+ storage behavior [13–15]. These inherent characteristics provide HC with strong potential to enhance the overall electrochemical performance of PIB systems. However, pristine HC still faces several limitations, such as relatively poor electronic conductivity and noticeable capacity decay at high current densities [16,17]. These drawbacks mainly arise from insufficient electrical conductivity, which restricts rapid ion/electron transport during high-rate cycling, as well as the limited number of accessible K^+ storage sites, ultimately constraining capacity under fast charge–discharge conditions. Although approaches including conductive additive incorporation, pore structure optimization, and surface engineering have shown some improvements, heteroatom doping offers a more fundamental and versatile solution. By tuning the electronic structure and local chemical environment of the C framework at the atomic level, heteroatom doping can simultaneously enhance conductivity, create additional active sites, and promote faster ion diffusion. Furthermore, the synergistic effects introduced by multi-heteroatom doping further improve these properties, making heteroatom engineering an effective and widely adopted strategy for optimizing HC anodes.

To overcome the inherent limitations of HC, significant research efforts have focused on heteroatom doping as an effective modification approach, leading to remarkable progress in recent years [18–20]. Due to the differences in atomic radius and electronegativity between heteroatoms and C atoms (Figure 1a), the introduction of dopants induces pronounced changes in the physicochemical properties of the C framework. These changes include modulation of the electronic structure, redistribution of charge density, variation in surface polarity, and the creation of structural defects, all of which strongly affect electrochemical performance [21–23]. In particular, heteroatom doping increases the number of electrochemically active sites, enhances electronic conductivity, and accelerates charge-transfer kinetics, thereby significantly improving the electrochemical behavior of C-based materials [24–26]. For instance, nitrogen (N) and sulfur (S) doping are known to facilitate electron transport and ion diffusion, whereas phosphorus (P) doping can effectively improve capacity by strengthening the C framework and introducing additional K-storage sites [27–29].

Accordingly, a variety of heteroatom species have been introduced to address the intrinsic limitations of pristine HC. With continuous progress in this field, doping strategies have gradually evolved from single-element modification to multi-element co-doping. Although individual dopants can selectively improve certain properties, for example, enhanced electronic conductivity through N doping or increased capacity through P incorporation, single-element doping rarely provides a balanced combination of high capacity, excellent rate capability, and long-term cycling stability. In contrast, multi-element doping utilizes

synergistic interactions among different heteroatoms to create an optimized electrochemical environment that surpasses the performance of single-doped systems. Rationally designed dopant combinations can simultaneously regulate charge transport, enlarge interlayer spacing, generate favorable K-adsorption sites, and enhance structural stability, thereby overcoming the limitations of single-doped configurations. Furthermore, multi-element co-doping not only improves electrical conductivity and structural robustness through combined effects but also enables precise tuning of K^+ storage sites [30,31]. The interaction between different dopant species creates a more favorable thermodynamic and kinetic environment for K^+ insertion/extraction, resulting in significant improvements in both capacity and cycling durability of HC materials. As illustrated in Figure 1b, heteroatom-modified HC offers multiple advantages, including improved electrical conductivity, expanded interlayer spacing, enhanced capacity, better electrolyte wettability, superior rate capability, extended cycle life, reduced cost, improved scalability, and effective suppression of dendrite formation.

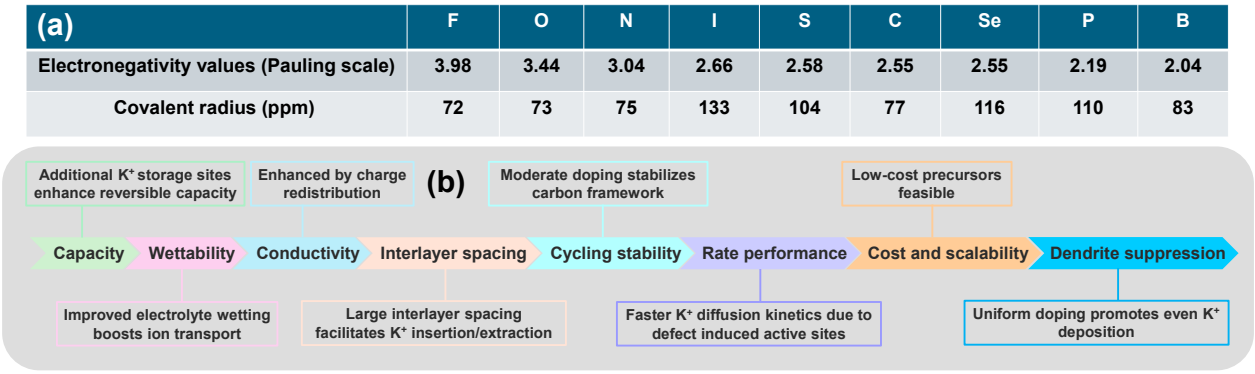

Figure 1. (**a**) Comparison of electronegativity (Pauling scale) and covalent radii (pm) of various heteroatoms. (**b**) Summary of the key benefits conferred by heteroatom doping on HC.

This review presents a detailed summary of recent progress in heteroatom-doped HC, with particular focus on the transition from single-element doping to multi-element modification strategies and their significant impact on electrochemical performance. The underlying mechanisms and the effectiveness of various doping methods in improving PIB performance are systematically discussed, followed by an evaluation of the remaining challenges and future research opportunities. In comparison with single-dopant systems, multi-element doping exhibits clear advantages in enhancing electronic conductivity, strengthening structural stability, and optimizing K-storage behavior, thereby overcoming the intrinsic limitations of pristine HC. Overall, the rational design of dopants in HC represents a promising strategy for developing high-performance PIB anodes and advancing next-generation battery technologies.

2. Basic Concepts and Working Principle of PIBs

As shown in Figure 2a, K possesses unique physical and economic advantages over Li and Na, making PIBs attractive candidates for next-generation energy-storage systems [32,33]. Furthermore, the fundamental working principle of PIBs is similar to that of LIBs [34,35]. As illustrated in Figure 2b, the electrochemical process relies on the reversible migration of K^+ ions between the cathode and anode. During charging, K^+ ions are extracted from the cathode and inserted into the anode, whereas the opposite process occurs during discharge. At the same time, electrons flow through the external circuit, producing usable electrical energy.

(a)	Potassium-ion batteries	Lithium-ion batteries	Sodium-ion batteries
Atomic radius (pm)	243	167	190
Ionic radius (Å)	1.38	0.76	1.02
Covalent radius (pm)	203	128	166
Voltage (V)	−2.93	−3.04	−2.71
Atomic number	19	3	11
Abundance (ppm)	25,900	20	28,300
Atomic weight (g mol^{-1})	39.09	6.94	22.99
Cost (USD/mt)	20,000	80,000	6000

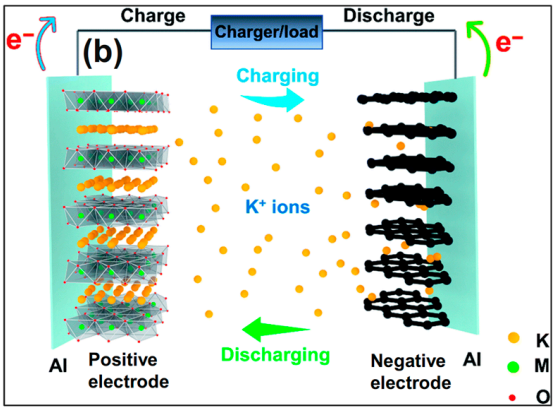

Figure 2. (**a**) Comparison of the main physical properties and economic factors of Li, Na and K. (**b**) Pictorial illustration of operating mechanism of PIBs.

Beyond differences in elemental abundance, PIBs, SIBs and LIBs also differ fundamentally in their electrochemical characteristics. Owing to the significantly larger ionic radius of K^+ compared with Li^+ and Na^+, K-ions exhibit much slower diffusion kinetics within solid electrode structures. This large size also results in poor compatibility with conventional LIB and SIB electrode materials.

Conventional cathode materials such as $LiCoO_2$ and typical anodes like graphite show limited structural stability during K^+ intercalation. Graphite, in particular, experiences severe volume expansion and delivers relatively low reversible capacity when accommodating K-ions. Consequently, the development of high-performance PIBs relies on electrode materials specifically designed for K-storage, including open-framework cathodes and disordered HC anodes with enlarged interlayer spacing. These structures are better suited to accommodate the large ionic radius of K^+ while mitigating kinetic constraints and mechanical stress [36,37]. The electrochemical performance of PIBs, including energy density, cycling stability, and rate capability, is strongly influenced by electrode architecture, reaction kinetics, electrolyte composition, and interfacial stability [38,39]. Therefore, systematic optimization of electrode materials, electrolyte systems, and electrode-electrolyte interfaces is essential for achieving high-performance PIBs.

3. Hard Carbon

Hard carbon (HC) is generally defined as a non-graphitizable C material that retains a highly disordered structure even after high-temperature treatment (typically above 2500 °C). It consists of randomly oriented and stacked graphene-like layers with enlarged interlayer spacing (usually >0.36 nm) and abundant closed micropores. These structural features distinguish HC from graphitizable (soft) carbons, which can transform into well-ordered graphite under similar thermal conditions. HC has become one of the most extensively studied anode materials for PIBs due to its excellent structural stability and superior electrochemical performance compared with conventional graphite and other candidate anodes. In contrast to graphite, HC features a highly disordered and amorphous C framework with enlarged interlayer spacing and abundant microporosity, which enables effective accommodation of large K-ions. Furthermore, HC supports multiple K-storage mechanisms that together contribute to high reversible capacity, while its hierarchical porous structure helps to alleviate volume changes during repeated cycling. Compared with other anode candidates such as alloy-based materials, metal oxides, and soft C, HC also offers clear advantages in terms of cost-effectiveness and sustainability. Its large SSA and well-developed porosity facilitate rapid K-ion transport and promote the formation of a stable low-voltage plateau during cycling. HC is typically synthesized

through high-temperature annealing of C-rich precursors, which produces an amorphous framework with high SSA and abundant microporosity [40]. These structural features provide numerous electrochemically active sites for K-ion adsorption and storage. Moreover, HC is composed of disordered graphitic domains interconnected with microporous regions, which facilitate efficient potassiation and ion diffusion while buffering volume changes during repeated cycling, thereby enhancing cycling stability [41]. Owing to these structural advantages, HC exhibits stable voltage characteristics and excellent long-term electrochemical performance, highlighting its potential as a promising anode material for PIBs.

The K-storage in HC is typically attributed to two dominant processes: interlayer insertion and surface adsorption [42,43]. The former involves the incorporation of K^+ ions into enlarged interlayer gaps of C sheets or their filling of microporous regions, mainly occurring during the early stages of charging. In contrast, surface adsorption arises from electrostatic interactions between K-ions and the C surface, which contributes to reversible capacity and improved rate performance. Nevertheless, the much larger ionic radius of K^+, approximately 1.8 times that of Li^+, significantly influences ion transport, resulting in inherent kinetic constraints that limit electrochemical performance. Therefore, optimizing the pore architecture, SSA, and structural ordering of HC is essential to enhance K-storage and diffusion behavior. Although HC shows considerable promise as an anode material, its practical application is limited by inherent shortcomings, particularly its low electronic conductivity. This issue becomes more severe under high-rate cycling, leading to sluggish electrochemical kinetics [44–46]. To address this, HC is typically combined with conductive additives such as graphite or C black. However, the intrinsically slow diffusion of K-ions constrains the attainable capacity at high current densities, thereby restricting its use in high-power applications, including EVs and portable electronics. Moreover, repeated insertion and extraction of the relatively large K-ions induce significant volume changes in HC, which can result in structural degradation and the loss of conductive pathways, ultimately deteriorating cycling stability [47]. These challenges are generally more pronounced in HC than in graphite-based materials. Additionally, the nonuniform distribution of K-storage sites further limits capacity utilization and long-term electrochemical performance.

Compared with many alternative anode materials, HC demonstrates relatively stable electrochemical performance at low temperatures, as evidenced by its good cycling stability and capacity retention under such conditions. In contrast, alloy-type anodes, such as Sn- and Sb-based materials and their heterostructures, often suffer from significant volume expansion and structural degradation at low temperatures. The amorphous and porous nature of HC can effectively buffer these volume changes, allowing it to preserve structural integrity during repeated cycling [9,48]. Moreover, HC exhibits more favorable ion diffusion kinetics than metal compound anodes at low temperatures, owing to its disordered C framework, which provides flexible pathways for K-ion transport and suppresses phase separation typically observed in metal-based systems. However, the large ionic radius of K-ion still leads to sluggish diffusion under cold conditions, resulting in diminished capacity and energy efficiency. To address these limitations, strategies such as heteroatom doping, C structure engineering, and electrolyte optimization have been extensively explored [49,50]. These approaches aim to enhance electronic conductivity, increase capacity, and improve cycling stability, particularly under high current densities and low-temperature conditions. Despite these advancements, further optimization of HC is still required to satisfy the requirements of high-performance and sustainable PIB technologies.

4. Doping Strategies for HC Anodes in PIBs

Heteroatom doping has been extensively utilized as an effective approach to improve the electrochemical performance of HC anodes in PIB systems [51,52]. As shown in Figure 3, various heteroatoms, such as N, S, and P, have been incorporated into HC through single-, dual-, and ternary-doping strategies. These modifications aim to tune the physicochemical properties of HC, thereby enhancing its electrochemical performance, particularly with respect to capacity retention and cycling stability [53]. Notably, the doping concentration of heteroatoms plays a decisive role in regulating the electrochemical performance of HC anodes. An appropriate doping level can effectively tailor the electronic structure, increase defect density, and introduce abundant active sites for K-ion storage, thereby enhancing capacity and rate capability. However, insufficient doping may not induce significant improvements, while excessive doping can disrupt the C framework, reduce electrical conductivity, and lead to structural instability during cycling. In several reported studies, optimized dopant contents have been shown to deliver superior performance compared to both low- and high-doping counterparts, highlighting the existence of an optimal doping range. Therefore, precise control of heteroatom content is essential for achieving a balance between conductivity, active site availability, and structural integrity.

4.1. Single-Element Doping

Single-element doping involves the intentional introduction of specific heteroatoms into the HC lattice to enhance its electrochemical performance in PIB systems. A wide range of dopant elements has been explored to regulate the physicochemical properties of HC. Through the creation of localized electron-rich or electron-deficient regions, heteroatom incorporation modifies the electronic structure of the C framework, thereby improving electrical conductivity and promoting more efficient electron transfer during charge–discharge processes [54,55]. These enhancements are particularly advantageous at high current densities, where rapid charge transfer is critical for achieving high reversible capacity. In addition to conductivity improvement, dopants can facilitate K-ion diffusion by tuning the local electronic environment and introducing additional active sites. Furthermore, heteroatom incorporation can mitigate volume changes during cycling, contributing to structural stability and improved cycling performance and capacity retention [56].

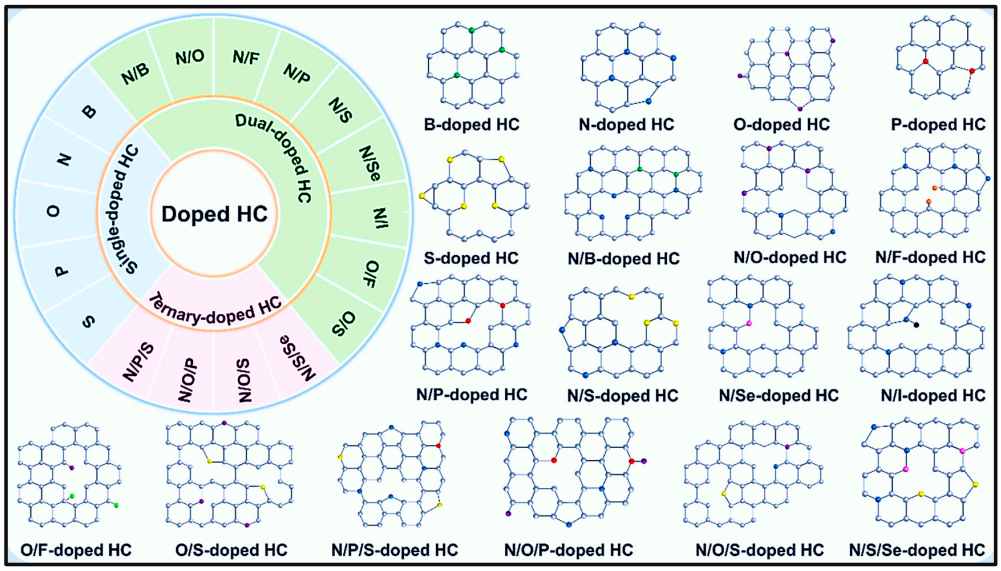

Figure 3. Pictorial representation of heteroatom-doping approaches and the corresponding structural configurations of doped HCs.

4.1.1. B-Doping

Boron (B) has been widely explored as an effective dopant for C-based materials due to its advantageous atomic properties [57]. Owing to its atomic radius being similar to that of C, B can be readily incorporated into the C lattice during the doping process [58]. As an electron-deficient element, B strongly modulates the electronic structure of C frameworks. Its incorporation activates otherwise inert π-electrons, introduces electron-deficient active sites, and facilitates charge transfer between K-ions and the C host. These electronic effects make B-doped C materials particularly promising for electrochemical applications. Notably, B acts as an electron acceptor within the conjugated C network, leading to charge redistribution and the formation of holes in the valence band. This, in turn, increases the local density of states (DOS) near the Fermi level, thereby enhancing electrical conductivity [59].

DFT calculations reveal that electron-deficient B-C sites serve as highly active centers for K-ion adsorption, significantly increasing the adsorption energy (E_{ads}) and promoting subsequent ion intercalation [60]. Wen's group [61] reported the synthesis of B-doped pinecone-derived C (BZPC) via high-temperature treatment in molten $ZnCl_2$, resulting in a 3D hierarchical porous structure. This architecture improves electrolyte wettability and charge-transfer kinetics, buffers volume changes during cycling, and offers abundant microporous sites for efficient K-ion adsorption. Raman spectroscopy indicated that BZPC possesses a higher I_D/I_G ratio (1.03) than undoped ZPC (0.89), suggesting increased defect density and structural disorder induced by B doping, which is advantageous for K-ion adsorption and diffusion. As an anode material for PIBs, BZPC delivered a reversible capacity of 223.8 mAh g^{-1} at 0.05 A g^{-1}, along with excellent rate capability and cycling stability, retaining 115.9 mAh g^{-1} after 2000 cycles at 1 A g^{-1}.

4.1.2. N-Doping

Nitrogen (N) doping significantly improves the energy storage performance of HC anodes in PIBs through multiple synergistic mechanisms. The electronegativity difference between N and C, together with the presence of various N configurations (graphitic, pyridinic, and pyrrolic), modulates the electronic structure of C framework. This modification reduces the band gap, enhances electron delocalization, and increases electrical conductivity. In addition, N doping introduces abundant K-ion storage sites, where pyridinic and pyrrolic N species, along with N-induced defects, lower the E_{ads} of K-ions and increase the density of active sites. These characteristics enable multiple storage pathways, including intercalation, surface adsorption, and pore filling. Furthermore, N incorporation tailors the microstructure by expanding interlayer spacing (0.36–0.4 nm) and creating hierarchical micro-/mesoporous architectures, which shorten ion diffusion distances and buffer volume variations during cycling. The presence of polar N-containing functional groups also improves electrolyte wettability and promotes the formation of a uniform and stable SEI. Meanwhile, strong C-N covalent bonds reinforce the structural integrity of the C matrix, preventing layer exfoliation and particle aggregation, thereby enhancing cycling stability. Collectively, these effects mitigate the inherent limitations of pristine HC, leading to improved capacity, rate performance, and long-term durability.

N-doped C (N-C) materials have shown great promise as anode candidates for PIBs. The incorporation of N enhances electronic conductivity and introduces abundant electrochemically active sites for K-ion adsorption, thereby promoting efficient charge-transfer processes. In addition, N doping improves structural stability by alleviating stress associated with volume changes during repeated cycling, leading to enhanced long-term performance [62,63]. Importantly, the benefits of N doping strongly depend on the bond-

ing configurations of N within the C matrix. Pyridinic N, which contains a lone pair of electrons, donates electron density to the C framework, elevates the Fermi level, and increases the local DOS, thereby improving conductivity [64]. In contrast, graphitic N mainly contributes to strengthening and stabilizing the C lattice. Computational studies further indicate that pyridinic N sites exhibit significantly higher adsorption affinity for K-ions than graphitic N configurations [65]. These defect-rich sites also lower the diffusion energy barrier for K-ion by approximately 0.2–0.3 eV, enhancing both thermodynamic and kinetic aspects of ion storage. Furthermore, the porous structure increases the SSA, providing additional pathways for reversible K-ion intercalation and ultimately improving overall storage capacity [66].

Furthermore, porous N-C materials offer several advantages, including low cost, environmental sustainability, and strong compatibility with diverse electrolytes, making them highly promising for PIB applications [67]. For instance, Xie and co-workers [68] reported porous N-C microspheres derived from chitosan (NCS, Figure 4a), which provide an efficient structural framework for K-ion storage. Remarkably, the material delivered a reversible capacity of 154 mAh g^{-1} even under demanding conditions, such as an elevated temperature of 72 °C and a high current density of 20 A g^{-1}. In addition, the NCS electrode exhibited outstanding cycling stability, with negligible capacity decay over 4000 charge–discharge cycles (Figure 4b). DFT calculations further indicated that N doping significantly enhances K-ion adsorption, while also improving electronic conductivity and ion transport. Coupled with the abundance and cost-effectiveness of chitosan, these properties highlight NCS as a highly promising anode material for PIBs.

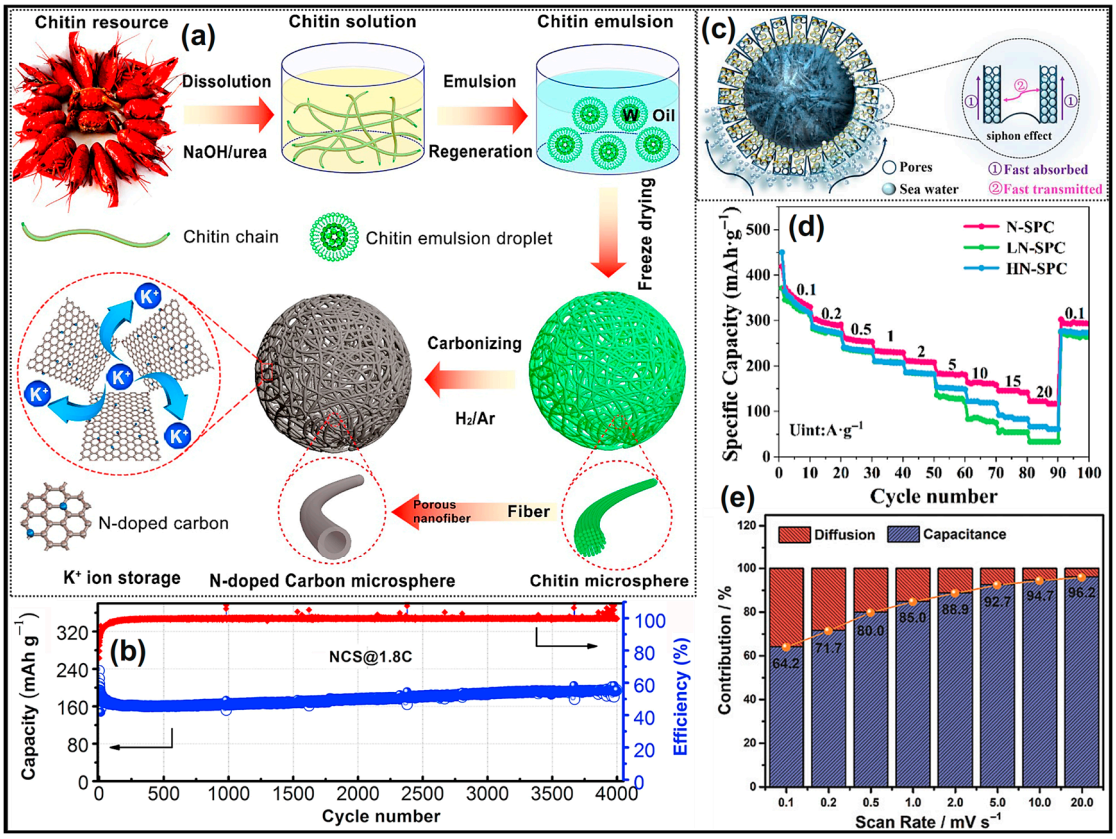

Figure 4. (**a**) Pictorial illustration of synthesis procedure for porous NCS. (**b**) Long-term cycling stability evaluation. Adapted [68]. Copyright 2017, Elsevier. (**c**) Diagram depicting siphon-type ion-transport behavior in porous sea-urchin-inspired spines. (**d**) Rate capability comparison of N-SPC, LN-SPC, and HN-SPC electrodes. Adapted [69]. Copyright 2021, Elsevier. (**e**) Capacitive contribution analysis of the NPC electrode at different scan rates. Adapted [70]. Copyright 2018, Wiley.

Huang's group [69] reported the synthesis of a sea urchin-inspired porous N-C material (N-SPC), designed by mimicking the unique architecture and efficient ion transport characteristics of natural sea urchins. This biomimetic structure generates a pronounced porous siphon effect and facilitates rapid ion kinetics (Figure 4c), enabling efficient K-ion insertion and extraction. The obtained N-SPC exhibits a high SSA, a hierarchical micro-/mesoporous structure, abundant N-induced defects, and reduced K-ion diffusion energy barriers. As a result, the material delivers excellent rate performance and cycling stability, maintaining a reversible capacity of 116 mAh g^{-1} even at an ultrahigh current density of 20 A g^{-1} (Figure 4d). Furthermore, when assembled into a full cell with a Prussian blue (PB) cathode, the device achieves a capacity of 113 mAh g^{-1} at 0.47 A g^{-1} over 100 cycles, highlighting its potential for practical energy storage applications.

Ci and colleagues [70] proposed a facile and effective approach to synthesize layered porous N-C (NPC). When evaluated as an anode for PIBs, the NPC demonstrated remarkable electrochemical performance along with excellent cycling durability. CV analysis revealed that K-ion storage is predominantly governed by surface-controlled capacitive processes, with the capacitive contribution increasing from 64.2% at 0.1 mV s^{-1} to 96.2% at 20 mV s^{-1} (Figure 4e). Moreover, the NPC electrode exhibited low charge-transfer resistance (R_{ct}) and negligible capacity decay over 500 cycles. DFT calculations indicated that pyridinic-N and pyrrolic-N sites possess stronger K-ion adsorption capabilities, with adsorption energies of −2.68 and −2.38 eV and shorter adsorption distances of 0.28 and 0.26 nm, respectively, compared to pristine graphene (−1.93 eV). These findings confirm the enhanced K-affinity induced by N-doping. Additionally, DOS analysis revealed increased electronic conductivity near the Fermi level in N-C materials, highlighting the positive role of N incorporation in facilitating charge transfer. Overall, this study not only demonstrates the advantages of porous N-C materials for PIBs but also provides valuable insights into K-ion storage mechanisms at heteroatom-modified active sites, offering guidance for the rational design of advanced PIB electrodes.

In comparison with other porous C materials, mesoporous C exhibits unique advantages. The presence of mesopores provides efficient channels for mass transport, enabling improved electrolyte infiltration and faster ion diffusion, which significantly enhances electrochemical performance [71]. Additionally, precise control over mesopore size within the C framework can further improve ionic conductivity and interfacial wettability [72]. Recent work has reported mesoporous N-C spheres (MCS) with enlarged interlayer spacing, high SSA, and abundant N active sites. These features collectively promote K-storage by facilitating electrolyte access and accelerating ion adsorption kinetics [73]. The MCS-7-900 anode delivers excellent rate capability, achieving 107.9 mAh g^{-1} at 5 A g^{-1}, along with outstanding cycling stability, mainly due to a capacitive-dominated storage mechanism with limited diffusion constraints. DFT calculations further identify pyridinic-N and pyrrolic-N as the primary adsorption sites for K-ions. Furthermore, N-doped mesoporous HC (NMC) was synthesized using a size-controlled NaCl templating approach, where smaller templates resulted in reduced particle size and enhanced interparticle conductivity [74]. The combined effects of graphitic-N doping and an optimized mesoporous structure improve electron transport and 3D electrolyte penetration, promoting the formation of a stable SEI. As a result, the NMC anode exhibits a high reversible capacity of 323.5 mAh g^{-1} and maintains 292.7 mAh g^{-1} after 620 cycles.

Wu's team [75] fabricated mesoporous N-doped CNFs (NMCNFs) with interconnected hierarchical porosity via an electrospinning approach, employing renewable PAN-based acrylic yarn as both C and N sources. XPS survey spectra verified the presence of C 1s (285 eV), N 1s (400.1 eV), and O 1s (532.8 eV) peaks, confirming successful N incorporation

with a total content of 7.98%. High-resolution N 1s analysis revealed that pyridinic-N (398.2 eV) and pyrrolic-N (399.8 eV) were the dominant N species, contributing 41% and 48.9% of the total N, respectively, which enhances K-ion adsorption stability. Owing to the synergistic combination of hollow fibrous structure, high SSA, and abundant pyridinic/pyrrolic sites, the optimized NMCNFs exhibit superior K-storage performance, delivering 351.1 mAh g^{-1} at 0.2 A g^{-1} after 500 cycles and maintaining 122.3 mAh g^{-1} after 20,000 cycles at 5 A g^{-1}. DFT calculations further attribute the enhanced electrochemical behavior to shortened ion diffusion pathways, defect-rich active sites, and strengthened K-ion adsorption induced by N doping.

HC, characterized by its disordered microstructure, is widely considered a promising anode material for PIBs. However, the pronounced structural disorder typically leads to low electronic conductivity, which limits its rate performance [76]. Recent advances suggest that regulating the C microstructure through controlled graphitization can produce a hybrid framework consisting of conductive graphitic domains embedded within an amorphous matrix, thereby enhancing electrical conductivity and overall electrochemical performance [77]. This strategy effectively overcomes conductivity-related limitations while retaining the inherent advantages of HC. In this context, Zhang's group [78] reported the preparation of partially graphitized N-doped HC (NGHC) with a well-designed architecture incorporating mesoporosity, N doping, and uniformly distributed graphitic regions. The combined effects of these features significantly improve electron transport and reaction kinetics, resulting in enhanced electrochemical performance. Ex situ Raman spectroscopy indicates that K-ion storage in NGHC mainly follows an adsorption-insertion mechanism. Furthermore, full-cell evaluations using PTCDA as the cathode confirm the practical applicability of NGHC for PIB systems.

Chen and co-workers [79] developed a sustainable and scalable approach to synthesize N-doped HC (NHC) anodes using waste corn stover as a renewable C source. The synthesis process involved a urea-assisted pretreatment followed by controlled pyrolysis, yielding NHC with a high K-storage capacity of 402 mAh g^{-1}. High-resolution N 1s XPS spectra revealed three types of N species, among which graphitic-N (401.2 eV) was dominant. As a result, the NHC exhibits a relatively high degree of graphitization, with approximately 87% of the total capacity contributed from the low-voltage region below 1 V. Kinetic analysis suggests that K-ion storage is primarily governed by a diffusion-controlled intercalation mechanism. This study not only presents an efficient route for fabricating high-performance PIB anodes but also highlights the potential for sustainable utilization of agricultural waste.

4.1.3. O-Doping

Oxygen (O) incorporation has been shown to significantly improve the wettability of HC electrodes, thereby facilitating electrolyte penetration and enhancing ion transport within the electrode, which ultimately leads to improved electrochemical performance [80]. Furthermore, the introduction of O-functionalities into the C framework generates additional active sites and enhances interfacial reactivity, contributing to increased K-ion storage capacity and better PIB behavior [81]. Liu et al. [82] reported a porous HC (P-HC) electrode synthesized via a molecular-level design strategy, resulting in an in situ constructed C framework with uniformly distributed pores and engineered defect sites (Figure 5a,b). This well-defined structure effectively promotes electrochemical activity and ion diffusion. Electrochemical testing shows that the P-HC electrode delivers a reversible capacity of 328.7 mAh g^{-1} after 100 cycles at 0.1 A g^{-1}. Moreover, it exhibits excellent long-term cycling stability, maintaining stable capacity over 2500 cycles at 1 A g^{-1} (Figure 5c). The superior performance is primarily attributed to the uniform porous architecture and enhanced charge-transfer kinetics induced by O-doping.

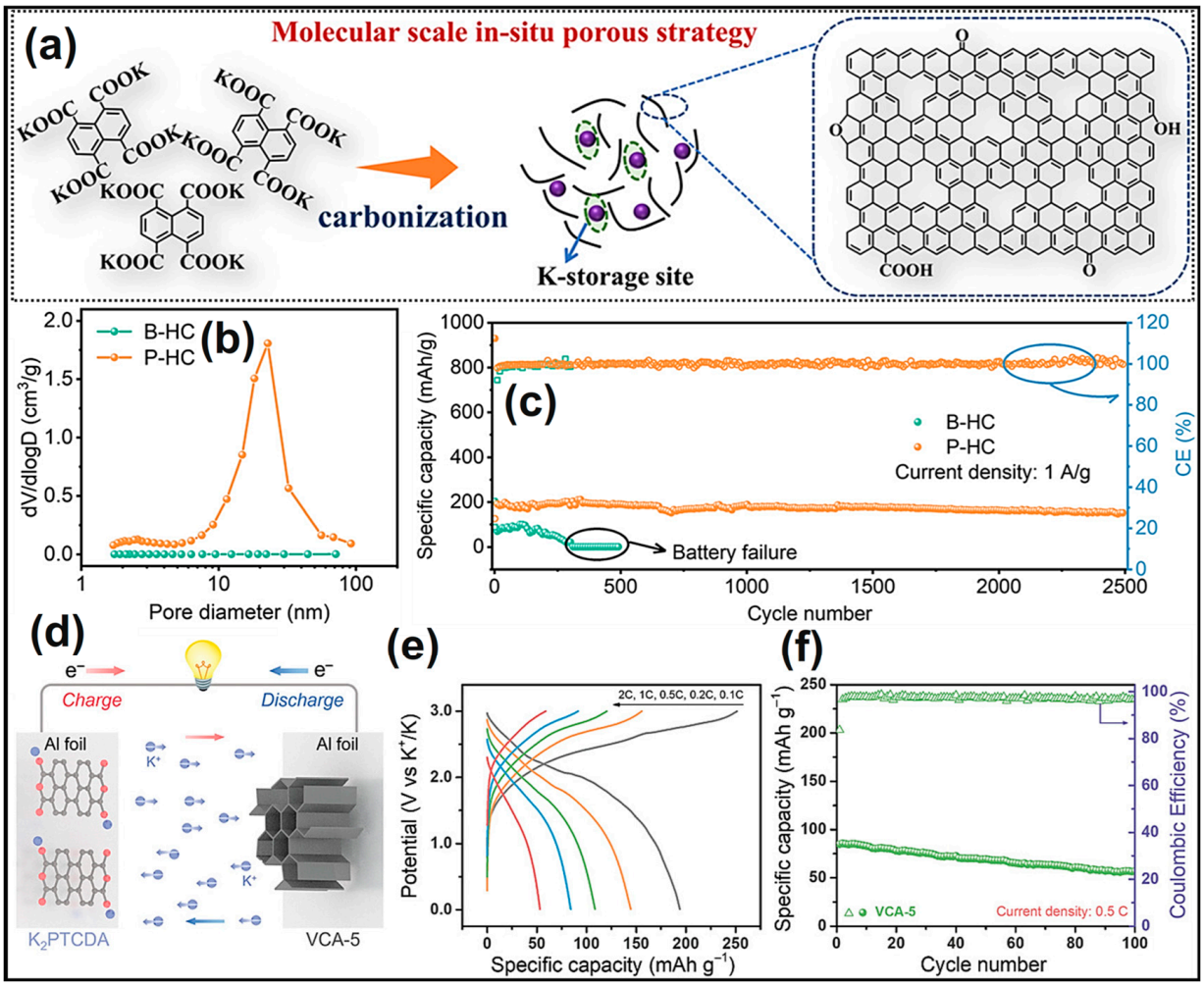

Figure 5. (**a**) Schematic demonstration of synthesis process for P-HC. (**b**) Comparison of pore size distributions of bulk HC (B-HC) and P-HC. (**c**) Cycle behavior of P-HC electrode. Adapted [82]. Copyright 2023, American Chemical Society. (**d**) Pictorial representation of working mechanism of PIBs. (**e**) Charge–discharge voltage profiles. (**f**) Cycle behavior of full cell device. Adapted [83]. Copyright 2022, Wiley.

Stephen's team [83] reported the fabrication of O-incorporated vertically aligned C aerogels (VCAs) using a precisely controlled 1D ice-templating technique. The resulting lamellar porous structure offers continuous channels that facilitate rapid ion transport and effective electrolyte infiltration. The VCA-5 anode exhibits excellent electrochemical performance, delivering a capacity of 258 mAh g^{-1} at 0.1 C and retaining 82.7% of its initial capacity after 1000 cycles at 0.5 C. Moreover, a full cell assembled with a K_2PTCDA cathode achieves an energy density of 118 Wh kg^{-1} along with stable cycling performance (Figure 5d–f). These findings demonstrate the strong potential of C aerogels for advanced K-ion storage and highlight the effectiveness of ice-templating in constructing well-defined porous architectures. The engineered electrode framework shortens ion diffusion pathways while enhancing structural stability, representing a significant advancement in electrode design.

4.1.4. P-Doping

Although phosphorus (P) doping has been widely utilized to modify the properties of C materials, its exact effects on the structural features of HC and its contribution to alkali metal ion storage are not yet fully clarified. Therefore, establishing a controllable strategy

for P incorporation and systematically investigating the corresponding electrochemical mechanisms are essential for the development of high-performance alkali-ion battery anodes. Yong and co-workers [84] introduced a cost-effective method to synthesize P-doped HC (PHC-700) via crosslinking epoxy resin with H_3PO_4, followed by heat treatment (Figure 6a). In this process, H_3PO_4 acts both as a crosslinking agent and a P source, facilitating effective P integration into the C matrix. The obtained PHC-700 exhibits advantageous structural features, including enlarged interlayer spacing, abundant P-C bonding, reduced SSA, and enhanced graphitic ordering. Moreover, the coexistence of P-O and P-C bonds provides additional active sites for K-storage, thereby improving electrochemical performance. Notably, the chemical configuration of P plays a critical role; highly polar P-O bonds create localized electropositive regions that enhance interactions with K-ions through Coulombic forces. In contrast, P-C bonds are directly embedded within the C framework, leading to slight lattice distortions and the formation of topological defects that act as low-energy channels for ion diffusion. The synergistic effect of strong K-ion adsorption induced by P-O bonds and improved ion transport enabled by P-C bonds results in concurrent enhancement of both capacity and rate performance. Electrochemical testing shows that PHC-700 achieves a reversible capacity of 381.9 mAh g^{-1} at 0.1 A g^{-1} and retains 260 mAh g^{-1} after 1000 cycles at 0.2 A g^{-1} (Figure 6b). Moreover, in situ NMR analysis confirms that both P-O and P-C bonds participate in K-ion adsorption, with P-C bonds dominating the redox reactions, thereby significantly improving overall electrochemical performance and rate capability (Figure 6c).

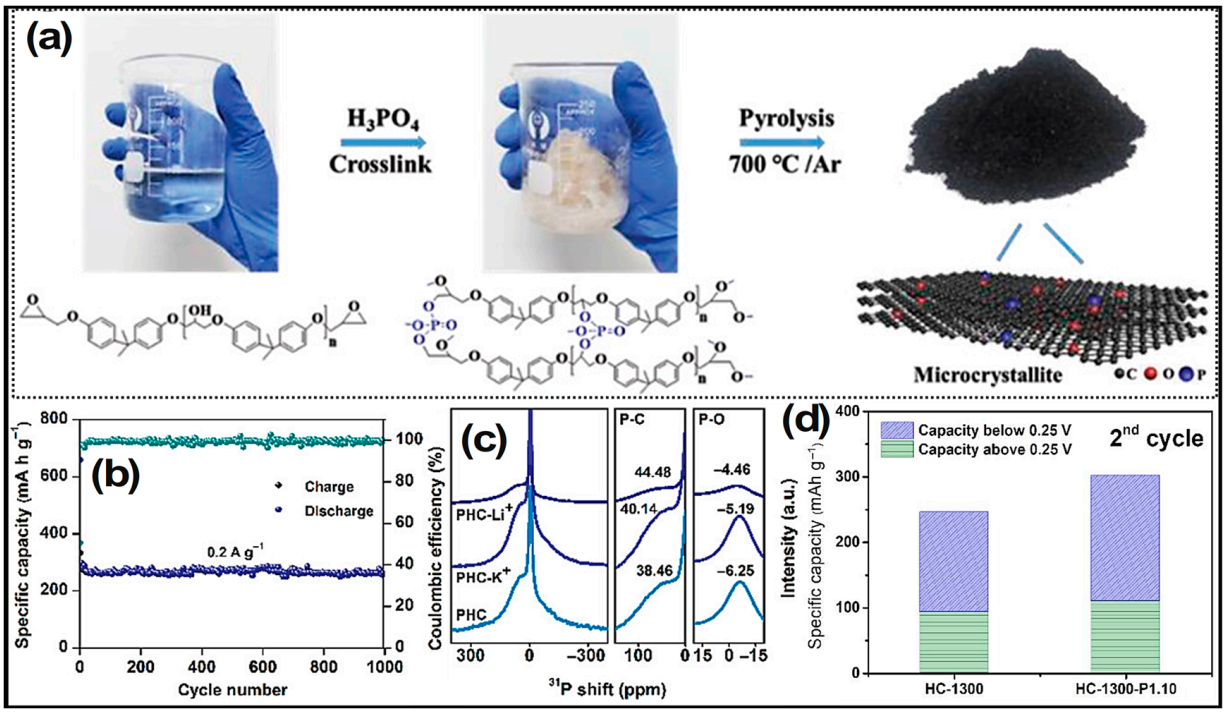

Figure 6. (**a**) Schematic illustration of synthesis procedure and microstructural characteristics of PHC-700. (**b**) Long-term cycle behavior of PHC-700. (**c**) In situ NMR analysis. Adapted [84]. Copyright 2019, Wiley. (**d**) Comparison of plateau capacities. Adapted [85]. Copyright 2020, Elsevier.

Moreover, the introduction of P significantly improves the structural integrity and interfacial stability of the C framework, resulting in outstanding long-term cycling performance. To further enhance the capacity contribution in the low-voltage region, a lignin-derived P-doped HC was prepared via pyrolysis at 1300 °C [85]. Compared with the undoped sample, the P-modified electrode exhibits markedly improved electrochemical performance

in PIBs, delivering a capacity of 302 mAh g^{-1}, which corresponds to an increase of 23%. In particular, the low-voltage capacity rises from 153 to 192 mAh g^{-1}, while the total capacity increases from 245 to 302 mAh g^{-1}. These results highlight the key role of P incorporation in modulating K-storage behavior and improving overall energy density (Figure 6d). Overall, controlled P doping in lignin-derived HC represents an effective strategy for developing low-cost, high-energy-density PIB anodes.

4.1.5. S-Doping

Sulfur (S) doping is widely recognized as an effective approach to enhance the performance of C-based anodes in PIBs, mainly by increasing capacity and improving electrochemical kinetics [86]. Due to its unique physicochemical properties, such as relatively high electronegativity and large atomic size, S can reversibly interact with K-ions, thereby contributing to enhanced storage capacity [87]. The difference in electronegativity between S and C generates polarized active sites within the C framework, facilitating K-ion adsorption. In addition, the larger atomic radius of S leads to expanded interlayer spacing, which alleviates structural stress during K-ion insertion/extraction and promotes ion diffusion [88]. Beyond structural effects, S incorporation also modifies the electronic structure by redistributing electron density. The participation of S p-orbitals introduces additional electronic states near the Fermi level, enhancing charge delocalization and electrical conductivity [89]. These combined structural and electronic effects significantly improve energy storage performance by increasing active sites and accelerating K-ion transport kinetics [90].

For example, Sun's team [91] proposed a facile synthetic approach for the preparation of S-containing porous hollow C spheres (SHPCS) with adjustable S content (Figure 7a). Structural analyses reveal that the introduction of S effectively tailors the C framework and enhances the availability of electrochemically active sites. At an optimal S level, the SHPCS electrode exhibits excellent electrochemical performance, delivering a capacity of 454 mAh g^{-1} at 0.05 A g^{-1}. Remarkably, it retains 211.4 mAh g^{-1} after 1000 cycles at 1 A g^{-1}, corresponding to a high-capacity retention of 93.7%.

To gain deeper insight into the influence of S doping configurations on electrochemical performance, DFT calculations were conducted to evaluate the E_{ads} of K-ions on two representative S-doped structures. As shown in Figure 7b,c, the trisulfur-doped configuration with vacancies (3S-V) exhibits stronger interaction with K-ion compared to the monosulfur-doped structure (1S). However, although heteroatom doping can enhance electrochemical properties, excessive incorporation may be detrimental. High S content can disrupt the conjugated C network, leading to decreased electrical conductivity. These negative effects arise from lattice distortions caused by differences in atomic size and electronegativity, which hinder electron transport and compromise structural stability during long-term cycling. Therefore, precise control of the doping level is crucial to achieve an optimal balance between electrochemical performance, conductivity, and structural integrity [92].

For example, a S-rich hollow C material (SHC-3) with a S content of 27.05 wt % was prepared using polystyrene and S as precursors [93]. When employed as an anode in PIBs, SHC-3 exhibits excellent cycling stability and rate capability. It delivers a reversible capacity of 298.1 mAh g^{-1} at 0.1 A g^{-1} and retains 95.2% of its capacity after more than 1000 cycles. Even at a higher current density of 0.5 A g^{-1}, a capacity of 220.2 mAh g^{-1} is maintained with outstanding stability over 5200 cycles. Structural and kinetic analyses reveal that the enlarged interlayer spacing of SHC-3 promotes rapid K-ion diffusion, alleviates mechanical stress during repeated cycling, and preserves structural integrity. Furthermore, DFT calcu-

lations indicate that S incorporation introduces abundant K-ion adsorption sites, thereby enhancing reversible K-storage capacity in PIBs.

The electrochemical characteristics of PIBs, including capacity, rate capability, and cycling stability, can be significantly improved through precise regulation of S doping. In this context, Fan's group [94] employed polythiophene (PTh) as a C precursor, which upon pyrolysis yields S-rich, sp^2-dominated C frameworks. By optimizing the carbonization temperature to 700 °C, the obtained S-doped HC (SC-700) maintains both high S content and adequate electrical conductivity (Figure 7d). The SC-700 electrode delivers a reversible capacity of 442 mAh g^{-1} at 0.05 A g^{-1}, retains 162 mAh g^{-1} at 10 A g^{-1}, and exhibits excellent cycling stability. Raman and XPS analyses indicate that an optimal S concentration can simultaneously enhance pseudocapacitive contributions and accelerate K-ion intercalation kinetics while preserving good electronic conductivity. Furthermore, S doping effectively modulates intrinsic defect structures and microstructural features, thereby influencing K-storage pathways. Therefore, careful control of defect density combined with appropriate S content is essential for achieving high capacity and stable cycling performance.

To elucidate the K-storage mechanism, Huang and co-workers [96] synthesized porous S-doped C spheres (SPCS) with tunable defect densities and S contents by varying the carbonization temperature. Pronounced structural differences were observed under different thermal conditions. An optimal combination of S concentration and defect density was identified, which promotes K-ion storage by enabling deeper intercalation, enhancing redox-related charge transfer, and increasing K-ion adsorption at active sites. The optimized SPCS electrode delivers a capacity of 435.1 mAh g^{-1} over 100 cycles at 0.05 A g^{-1}. Furthermore, in situ XRD analysis reveals that although the lattice becomes increasingly disordered during K-ion insertion, the interlayer spacing remains nearly unchanged, providing new insights into the structural evolution process.

The C structures rich in edge sites can significantly promote ion transport by shortening diffusion pathways, while expanded interlayer spacing facilitates reversible ion insertion and extraction, collectively improving electrochemical performance [97,98]. Based on this concept, S-doped C rods (SCNs) featuring abundant edge planes, incorporated S species, and high aspect ratios were synthesized [99]. The rod-like morphology exposes a large number of active edge sites to the electrolyte, thereby reducing ion diffusion distances. When used as anodes in PIBs, the SCNs deliver a capacity of 300 mAh g^{-1} at 0.05 A g^{-1}, along with excellent rate capability and long-term cycling stability, retaining 81 mAh g^{-1} after 1000 cycles at 1 A g^{-1}. These findings highlight that precise regulation of dopant distribution is an effective strategy for developing high-performance PIB anodes.

Liu and co-workers [100] reported the synthesis of mesoporous S-doped C spheres (S-MCSs) with highly accessible internal SSA and excellent K-storage performance. By carefully controlling the level of S incorporation during preparation, the authors systematically examined the influence of different doping configurations on K-storage behavior. The results showed that S atoms inserted between C layers effectively enlarged the interlayer spacing and improved K-ion adsorption, thereby enhancing the electrochemical performance. The optimized S-MCS electrode delivered a capacity of 144 mAh g^{-1} at 5 A g^{-1} and achieved 325 mAh g^{-1} after 100 cycles at 0.1 A g^{-1}, corresponding to a capacity retention of 91.2%. DFT calculations further confirmed the important role of S-doped sites in regulating the energy-storage behavior. In addition, insufficient electrode-electrolyte wettability was identified as a key factor responsible for non-uniform current distribution, uneven interfacial reactions, and unstable SEI formation, which ultimately led to the deterioration of anode performance.

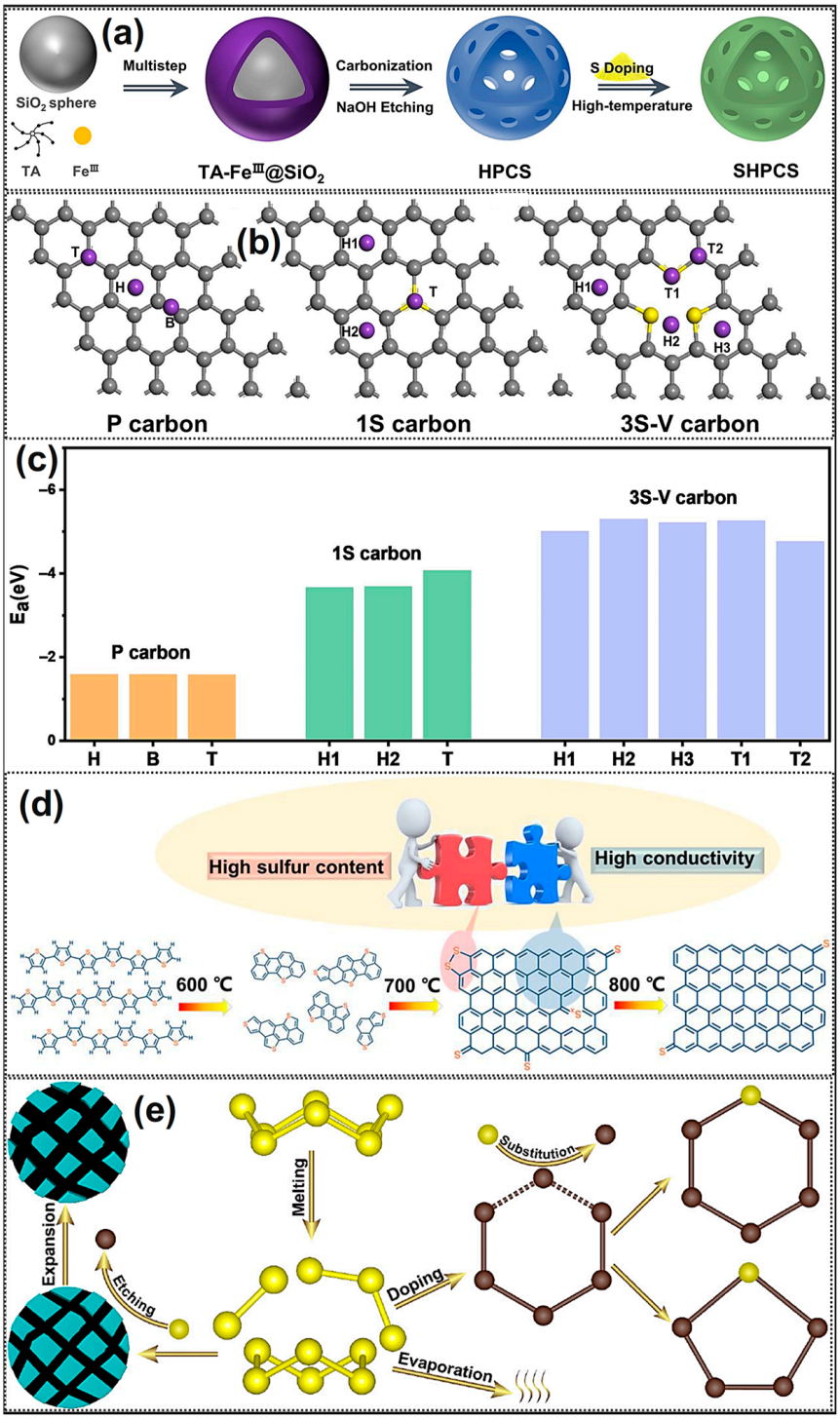

Figure 7. (**a**) Pictorial demonstration of the synthesis route for SHPCS. (**b**,**c**) Representative adsorption configurations and the associated energy barriers (E_a) for K^+ on P-, 1S-, and 3S-vacancy C models. Adapted [91]. Copyright 2023, Elsevier. (**d**) Illustration of the structural evolution pathway of Pth. Adapted [94]. Copyright 2023, Elsevier. (**e**) Schematic representation of the S-doping activity. Adapted [95]. Copyright 2022, American Chemical Society.

To address this limitation, Wang and colleagues [101] proposed a pore-engineering strategy to enhance electrolyte wettability and accelerate K-ion diffusion kinetics in HC. By constructing a tailored pore architecture, the obtained porous HC (HPC) exhibited improved capillary effects, which facilitated electrolyte infiltration, ensured uniform ion distribution, stabilized the SEI layer, and shortened ion diffusion pathways. In addition,

S doping increased ionic conductivity and introduced K-affinitive active sites within the C matrix, thereby improving the overall capacity. The resulting 2D sheet anode delivered 396.6 mAh g^{-1} after 200 cycles at 0.1 A g^{-1} and retained 122.9 mAh g^{-1} at 4 A g^{-1}. In situ TEM observations further confirmed that the mesoporous framework could accommodate volume variations more effectively than microporous carbons. This work demonstrates the close relationship between electrolyte wettability and K-ion transport kinetics and provides a practical strategy for designing high-performance PIB anodes.

A comprehensive understanding of S incorporation is essential for the rational design of S-doped C electrodes. Hou's group [95] systematically investigated the doping behavior of S and its influence on K-storage performance. The results revealed that, during high-temperature pyrolysis, S species can etch the C framework, resulting in increased microporosity and a lower degree of graphitization (Figure 7e). Raman analysis showed that the S-doped HC (SHC, 0.885) exhibited a higher I_D/I_G ratio than pristine HC (0.781), indicating the formation of additional defects induced by S incorporation. Consistently, XRD patterns of SHC displayed broader diffraction peaks, further confirming the reduced graphitic ordering. Meanwhile, part of the S atoms substituted C sites to achieve effective heteroatom doping, while the remaining S species were trapped within micropores, modifying both the pore structure and surface chemistry. Electrochemical measurements demonstrated that the SHC electrode delivered a capacity of 405.2 mAh g^{-1} at 0.05 A g^{-1} with stable cycling performance. This study clarifies the structural role of S and provides theoretical guidance for the rational design of advanced PIB anodes.

4.2. Dual-Element Doping

Dual-heteroatom incorporation refers to the simultaneous introduction of two different heteroatoms into the HC framework, which can synergistically improve electrochemical performance [102]. Compared with single-element doping, co-doping offers broader possibilities for optimization, as the complementary effects of different dopants enable simultaneous enhancement of properties that are typically difficult to balance, such as electrical conductivity, ion transport, capacity, and cycling stability [103]. By carefully selecting dopant pairs with cooperative functionalities, multiple performance parameters can be improved through a single modification strategy [104]. These improvements mainly arise from synergistic electronic interactions at the atomic scale.

In N/B co-doped systems, N acts as an electron donor that elevates the Fermi level, whereas B functions as an electron acceptor, introducing p-type carriers. The donor-acceptor coupling between these elements improves and balances the local DOS, resulting in quasi-metallic conductivity [105]. In addition to bulk electronic effects, the uneven charge distribution creates localized electric fields or dipoles that enhance K-ion adsorption and lower diffusion energy barriers via charge redistribution at active sites. Similarly, N/P co-doping enhances electrical conductivity while increasing the density of electrochemically active sites for K-storage. Moreover, synergistic interactions among dopants contribute to structural integrity by mitigating excessive disorder and inactive defect formation caused by over-doping [24]. As a result, dual-element doping simultaneously improves rate performance, reversible capacity, and cycling stability, highlighting its potential for practical PIB applications.

4.2.1. N and B Co-Doping

N and B, located adjacent to C in the periodic table, have similar atomic radii, which facilitates their incorporation into the C lattice. Their co-doping generates pronounced cooperative interactions: pyridinic N introduces defects and active sites, while B alters the electronic structure by shifting the Fermi level toward the conduction band, thereby en-

hancing electrical conductivity [106]. Using a self-templating strategy, Zhang's group [107] prepared porous N,B co-doped C bubbles (NBPC) (Figure 8a). The material exhibited high SSA, enlarged interlayer spacing, hierarchical porosity, and abundant active sites. As a PIB anode, NBPC delivered a capacity of 534 mAh g^{-1} at 0.1 A g^{-1}, maintained 218 mAh g^{-1} at 10 A g^{-1}, and retained 358.9 mAh g^{-1} after 3000 cycles (Figure 8b). Kinetic analysis revealed that charge storage was dominated by surface-controlled pseudocapacitive processes (Figure 8c). Moreover, the incorporation of metal single atoms at edge sites has been identified as an additional strategy to improve K-storage in HC.

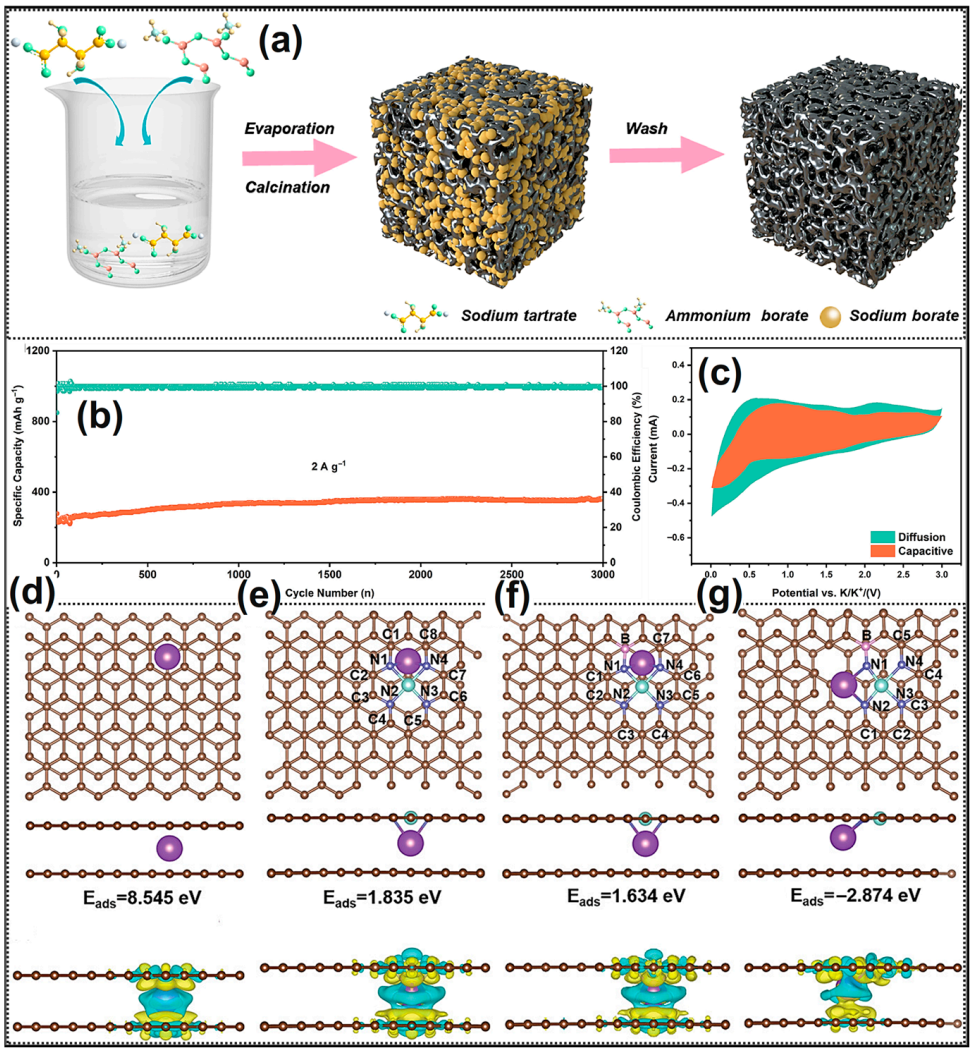

Figure 8. (**a**) Schematic illustration of the synthesis route for NBPC. (**b**) Cycling performance over extended cycles. (**c**) Contribution from pseudocapacitive storage. Adapted [107]. Copyright 2024, Elsevier. (**d**–**g**) DFT-calculated K atom adsorption on various structural models. Adapted [108]. Copyright 2023, Wiley.

Chen and co-workers [108] reported B,N co-doped CNTs featuring edge-anchored Ni-N_4-B configurations (Ni@BNHC), which exhibited outstanding K-storage performance. DFT calculations indicated that the coordination environment plays a decisive role in regulating interlayer K-storage behavior. Adsorption energy analysis showed that K-ion binding at edge Ni-N_4 sites (−2.874 eV) was significantly stronger than that on bilayer graphene (8.545 eV), in-plane Ni-N_4 (1.835 eV), and planar Ni-N_4-b (1.634 eV) structures (Figure 8d–g). In addition, the presence of isolated Ni atoms improved the reversibility

of K-storage at neighboring N/B sites, demonstrating the effectiveness of atomic-level coordination engineering in enhancing heteroatom-doped C anodes.

4.2.2. N and O Co-Doping

Metal–organic frameworks (MOFs) are crystalline porous materials distinguished by tunable pore structures, high SSAs, and ordered architectures [109,110]. These characteristics make them promising for energy storage and conversion applications [111,112]. C materials derived from MOFs generally retain high SSAs, appropriate porosity, and robust structures, which are advantageous for PIB systems [113,114]. Chen's team [115] synthesized mesoporous N/O co-doped C octahedra (MCOs) via calcination of Cu-BTC under a nitrogen atmosphere, followed by nitric acid treatment to remove residual copper and subsequent KOH activation. The superior electrochemical performance was attributed to the combined effects of high SSA, expanded interlayer spacing, and effective heteroatom doping. DFT results further indicated that the interaction between N and O dopants enhances electronegativity and conductivity, facilitating charge transfer.

To achieve both high capacity and excellent rate capability, Xiong and co-workers [116] synthesized N/O co-doped layered porous hydrocarbons (NOHPHC) for PIBs via controlled carbonization of NH_2-MIL-101 (Al), followed by acid etching. The NOHPHC anode exhibited reversible capacities of 365 mAh g^{-1} at 0.25 A g^{-1} and 118 mAh g^{-1} at 3 A g^{-1}, while retaining 69.5% of its capacity after 1100 cycles at 1.05 A g^{-1}. The superior performance was attributed to enlarged interlayer spacing that facilitates K-ion intercalation, a high SSA that enhances ion adsorption, and the cooperative interactions of N/O co-doping that accelerate charge transfer.

Simultaneously achieving high reversible capacity and fast charge capability remains a significant challenge for HC anodes in PIBs. To address this issue, Huang's team [117] developed 3D porous N/O co-doped HC hollow spheres (NO-HC) through combined structural engineering and heteroatom doping (Figure 9a). The material exhibits hierarchical micro- and mesoporous structures with gradient channels, which promote electrolyte penetration and accelerate K-ion diffusion. The incorporation of N and O expands interlayer spacing, improves K-ion insertion/extraction kinetics, and introduces additional adsorption sites. Ex situ XRD analysis revealed a reversible shift in the (002) peak to lower angles during discharge, indicating a synergistic adsorption-intercalation storage mechanism induced by heteroatom doping. Furthermore, controlled heat treatment led to in situ formation of graphitic domains within the amorphous C matrix, enhancing conductivity and providing extra K-ion storage sites (Figure 9b). As a result, NO-HC-600 delivered 234 mAh g^{-1} at 3 A g^{-1} and retained 98.82% capacity after 1200 cycles at 2 A g^{-1} (Figure 9c).

Biomass-derived C materials have attracted growing interest for energy storage applications due to their renewability, abundant availability, and low production cost [119]. Jiang's group [120] synthesized N/O co-doped HC by directly carbonizing sorghum stalk pith. The obtained material exhibited excellent PIB performance, maintaining a reversible capacity of 189.5 mAh g^{-1} after 5000 cycles at 1 A g^{-1}. This outstanding performance was attributed to the synergistic effects of a stable porous structure, enlarged interlayer spacing, and effective N/O heteroatom doping. The scalable synthesis approach highlights its potential for practical applications. Furthermore, the naturally hollow double-walled structure of Ganoderma lucidum spores provides a promising template for constructing novel C architectures.

Yao and co-workers [118] developed N/O co-doped amorphous biomass-derived caged C (NOBC). The hollow cage structure facilitates K-ion diffusion and adsorption, while the incorporation of N and O provides abundant active sites and enhances storage

capacity. The electrode delivered 334.6 mAh g^{-1} after 2000 cycles at 5 A g^{-1} and retained 124.19 mAh g^{-1} after 5000 cycles at 10 A g^{-1} (Figure 9d). These results highlight the effectiveness of utilizing natural biomass architectures to construct durable, high-performance electrodes and suggest promising pathways for sustainable energy storage.

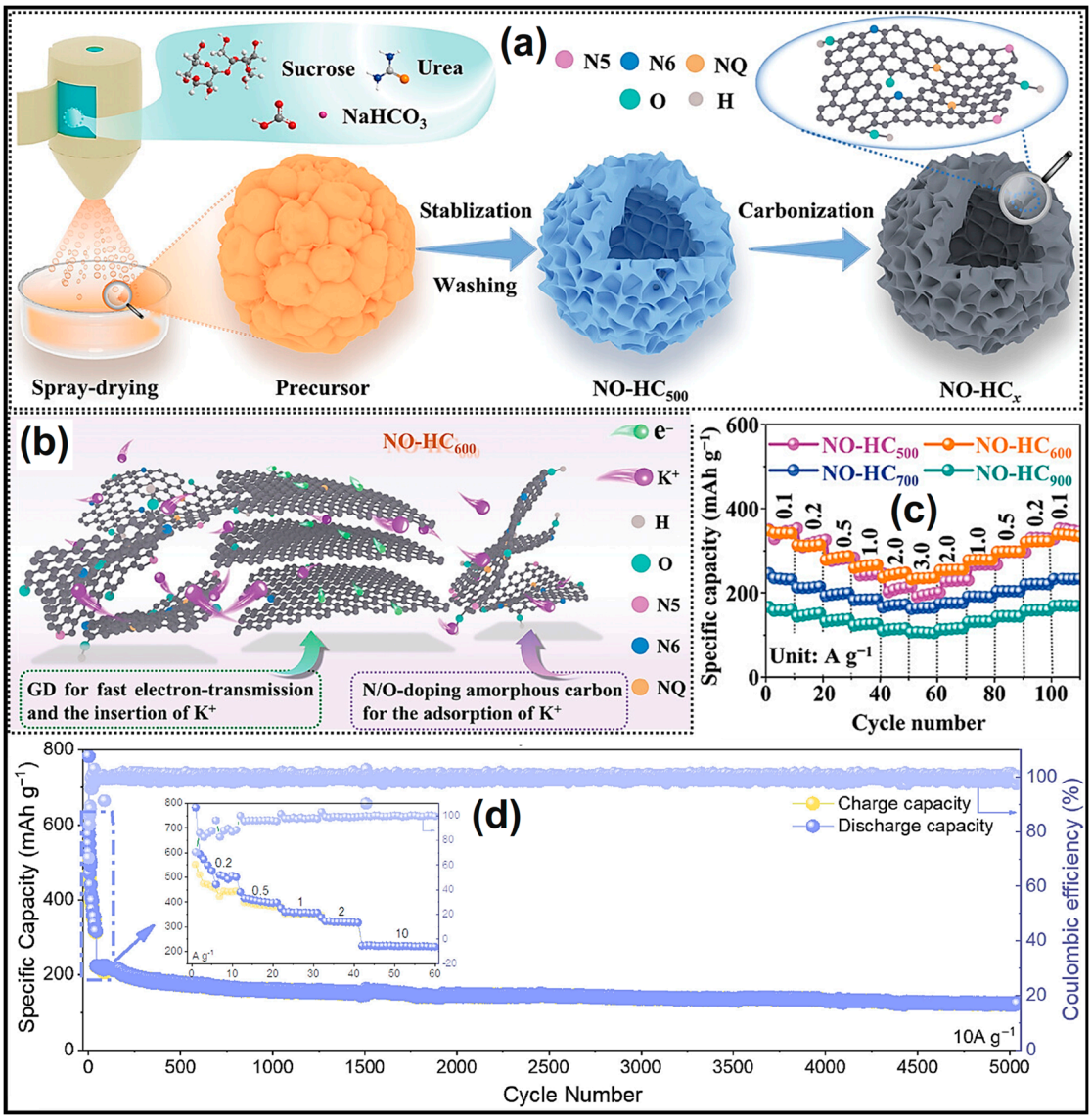

Figure 9. (**a**) Schematic demonstration of NO-HC_x preparation process. (**b**) Mechanistic representation of enhanced K^+ storage in NO-HC_{600}. (**c**) Rate capability. Adapted [117]. Copyright 2024, Wiley. (**d**) Cycling performance over prolonged operation. Adapted [118]. Copyright 2021, Elsevier.

4.2.3. N and F Co-Doping

Developing a controllable incorporation strategy that enables precise modulation of the E_{ads} of K-ion is of significant importance. To address this, an advanced heteroatom-doping approach has been proposed to finely tune the E_{ads} associated with K-ion adsorption. Using this method, N and F co-doped HC (N/F-HC) was synthesized via high-temperature treatment followed by an HF-assisted solvothermal process (Figure 10a) [121]. Experimental studies further demonstrated that uniform N/O co-doped C nanorods (CDC-900) could be prepared by carbonizing protein-rich porous cow dung-derived cellulose under optimized thermal conditions. A subsequent fluorination step enabled the selective substitution of surface $^{-}$OH and $^{-}$COOH groups with F atoms, resulting in the formation of CDCF-900. FTIR spectra confirmed successful F incorporation, as indicated by the emergence

of characteristic C-F (1079 cm^{-1}) and C-F_2 (1310 cm^{-1}) peaks, along with the weakening of $^{-}$OH and $^{-}$COOH signals. These observations suggest that F atoms preferentially replace O-containing functional groups during the doping behavior. Compared with N/O-doped C, N/F-doped HC exhibits more favorable K-ion Eads at defect sites, effectively reducing irreversible K-ion trapping. This controlled modulation suppresses undesirable electrolyte-electrode side reactions and promotes the formation of a uniform and stable SEI, thereby enabling faster K-ion transport during repeated cycling (Figure 10b). Further SEI analysis (Figure 10c) reveals that N/O-doped C tends to generate heterogeneous SEI layers, characterized by localized crystallization of inorganic species and unevenly passivated regions. In contrast, N/F doping leads to the formation of a more homogeneous SEI with a balanced distribution of inorganic and organic components. The uniformly dispersed inorganic phase enhances the mechanical strength of the SEI, while its high ionic conductivity facilitates rapid ion transport. Additionally, the interconnected 3D porous structure of CDCF-900 provides excellent rate capability and cycling stability, delivering a capacity of 214.2 mAh g^{-1} over 5000 cycles at an ultrahigh current density of 10 A g^{-1}.

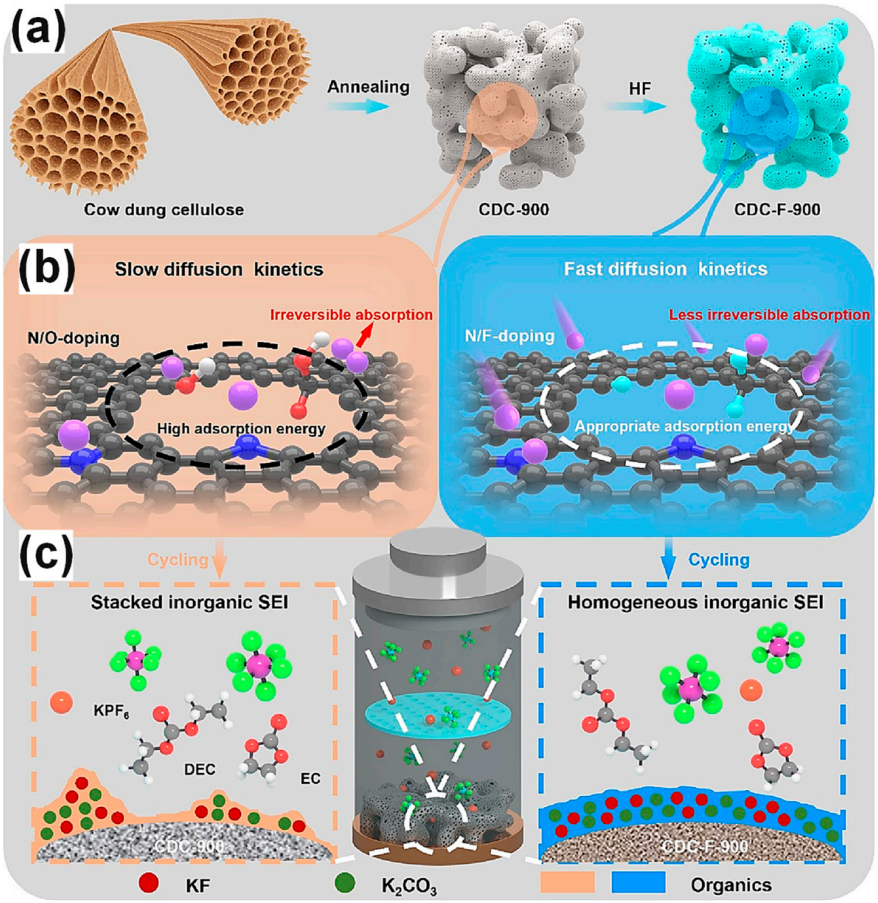

Figure 10. (**a**) Schematic illustration of preparation route for N/F doped HC. (**b**) Kinetic regulation of HC via E_{ads} tuning. (**c**) Relationship among SEI characteristics and reaction kinetics. Adapted [121]. Copyright 2024, Elsevier.

4.2.4. N and P Co-Doping

Compared with solely N-doped HC, the co-doping of P and N within C frameworks can further enhance PIB performance due to their synergistic interactions [122]. Recently, a facile method was reported for the fabrication of a self-supporting P/N co-doped C monolith (PN-PCM) [123]. The obtained PN-PCM features a distinctive 3D macroporous architecture with a honeycomb-like morphology, along with expanded interlayer spacing,

relatively low SSA, and high levels of P and N incorporation. The P content and its bonding configuration can be effectively regulated by adjusting the H_3PO_4 concentration during the phosphorylation process. When employed as a PIB anode, PN-PCM delivered a high reversible capacity of 396 mAh g^{-1} at 0.1 A g^{-1} and retained 168 mAh g^{-1} at 5 A g^{-1}, indicating excellent rate performance.

Wang et al. [124] reported the synthesis of a bowl-like C structure with dual N and P doping and a hierarchically porous framework, denoted as N/P-HPCB, for application as a PIB anode (Figure 11a). The N/P-HPCB electrode features a uniform distribution of heteroatoms, interconnected hierarchical porosity, and enlarged interlayer spacing, which collectively provide abundant active sites and facilitate rapid ion transport. Furthermore, the synergistic hollow-porous architecture effectively buffers volume changes during repeated potassiation and depotassiation, thereby improving mechanical stability. The self-stacked morphology enhances the continuity of conductive pathways, promoting efficient electron and ion transport. Consequently, the N/P-HPCB anode delivers a high reversible capacity of 458.3 mAh g^{-1} at 0.1 A g^{-1} and maintains stable capacity retention over 100 cycles (Figure 11b). Additionally, it exhibits excellent rate capability and long-term cycling stability while preserving its structural integrity during prolonged operation.

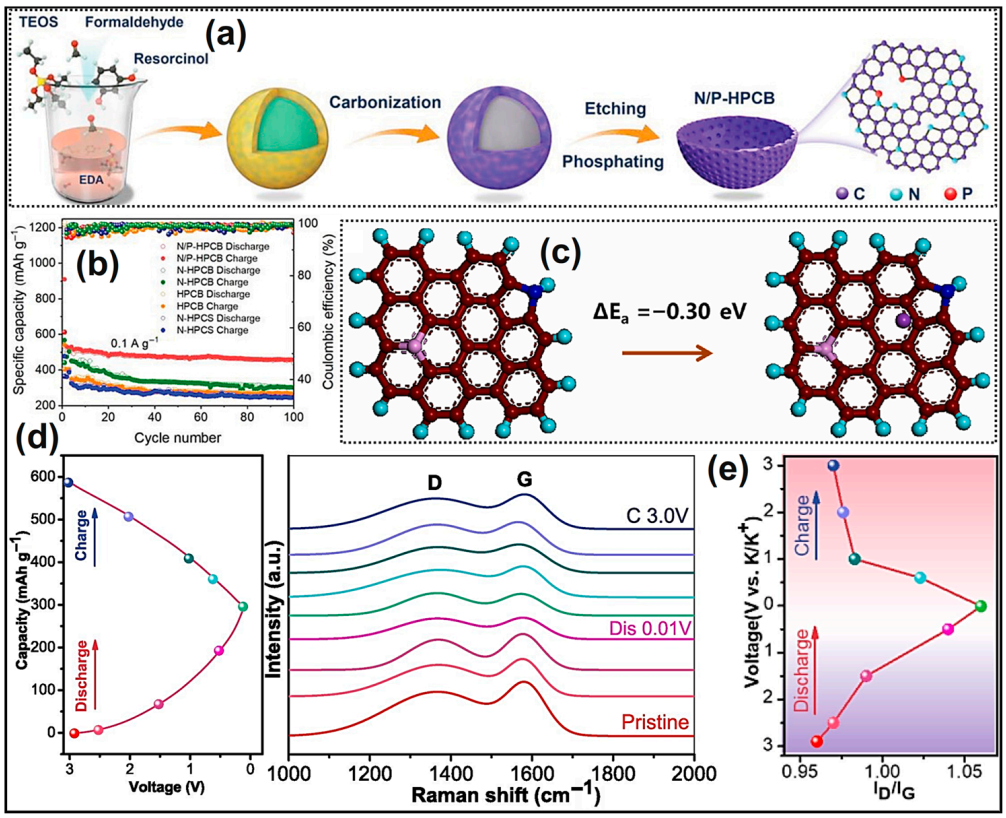

Figure 11. (**a**) Schematic representation of synthetic procedure for N/P-HPCB. (**b**) Cycling capability of the electrode. Adapted [124]. Copyright 2021, Wiley. (**c**) Structure of N and P incorporated HCNS-NP featuring pyrrolic-kind N. Adapted [125]. Copyright 2024, Elsevier. (**d**) Ex situ Raman spectra of N/P-HPCS at various electrochemical conditions, together with (**e**) relative evolution of the I_D/I_G ratio. Adapted [126]. Copyright 2022, Elsevier.

The electrochemical performance of N-C anodes is strongly influenced by the bonding configurations of N species within the C framework [127]. However, achieving precise control over electrochemically active sites, particularly pyridinic and pyrrolic N, remains a significant challenge. Recent progress in dual-heteroatom doping has provided effective

strategies for regulating these active configurations. Lyu's team [125] reported the synthesis of N and P co-doped hollow C nanorods (HCNS-NP) via controlled P incorporation (Figure 11c). XPS analysis of the N 1s region revealed three types of N species: pyridinic N (398.4 eV), pyrrolic N (400.9 eV), and graphitic N (402.4 eV). Compared with HCNS-N and HCNS-NS, the HCNS-NP sample showed a significant increase in pyrrolic N content accompanied by a decrease in pyridinic N, leading to an increase in the pyrrolic-to-pyridinic ratio from 1.6 to approximately 6. This observation suggests that P incorporation promotes the formation of pyrrolic N species. Consequently, the optimized HCNS-NP anode exhibits excellent K-ion storage performance, delivering 338.8 mAh g^{-1} at 0.1 A g^{-1} and maintaining 180.6 mAh g^{-1} at 1 A g^{-1} after 1000 cycles.

In a related study, Guo et al. [128] employed an alternative approach by constructing a 3D honeycomb-like C framework co-doped with P and N, specifically designed to enrich pyridinic N species. The hierarchically porous structure, abundant in defects and edge sites, provides a favorable environment for the formation of pyridinic N, while P incorporation enhances the exposure and accessibility of electrochemically active centers. This synergistic interplay between structure and composition facilitates rapid K-ion adsorption kinetics, resulting in a high-rate capability of 270.4 mAh g^{-1} at 1 A g^{-1}. Overall, these results demonstrate that controlled P/N co-doping enables selective modulation of N configurations to optimize K-storage behavior. In addition to specific N species, edge-located N atoms formed through substitution at defect sites within graphitic domains also play a crucial role in determining electrochemical performance.

Wang et al. [126] developed N/P-HPCSs, demonstrating that both structural engineering and P incorporation play critical roles in regulating edge N content and K-ion storage behavior. The pronounced nanoscale curvature of the hollow spheres significantly increases the exposure of edge-associated N sites. Simultaneously, P incorporation induces distortion in the graphitic lattice, further increasing the density of electrochemically active edge sites. Theoretical calculations reveal that the synergistic interaction between N and P enhances K-ion adsorption and optimizes the electronic structure, thereby enabling stable K-storage. Ex situ Raman spectroscopy was employed to monitor the structural evolution of the N/P-HPCS anode during electrochemical cycling. During potassiation, the I_D/I_G ratio gradually decreased (Figure 11d), which can be attributed to reduced optical penetration depth resulting from K-ion intercalation. Upon depotassiation, the Raman features were largely restored, indicating strong structural reversibility. The I_D/I_G ratio increased from 0.96 to 1.06 during discharge, reflecting increased structural disorder induced by K-ion insertion, and returned close to its original value during charging (Figure 11e), confirming a highly reversible storage process. Benefiting from its hollow architecture, the N/P-HPCS electrode effectively accommodates volume variations and enhances edge-site accessibility, delivering a capacity of 193 mAh g^{-1} at 4 A g^{-1}.

4.2.5. N and S Co-Doping

The simultaneous incorporation of N and S significantly modifies the electronic structure of HC, increases interlayer spacing, and introduces a high density of surface defects [129]. These combined effects contribute to enhanced K-ion storage capacity and improved charge-transfer kinetics [130]. Furthermore, the presence of a hierarchical porous structure creates 3D interconnected pathways that facilitate rapid K-ion diffusion and reduce ion transport resistance. Meanwhile, various biomass-derived and C-rich precursors, such as sorghum, lignite, and waste laboratory textiles, have been widely investigated as sustainable sources for fabricating HC anodes for PIBs.

Li and co-workers [131] reported the preparation of a nanostructured C material derived from sorghum biomass through mechanical processing, resulting in a unique

sheet-like morphology (Figure 12a). To further enhance electrochemical performance, N and S were simultaneously introduced during the carbonization process using thiourea as a dual-heteroatom precursor. The resulting N,S co-doped porous C (NSSC-600) exhibited excellent K-storage performance, delivering a capacity of 268 mAh g^{-1} at 0.1 A g^{-1}. DFT calculations revealed that N/S co-doping reduces the E_{ads} of K-ions, thereby facilitating faster ion adsorption and improving charge transport during intercalation and deintercalation.

Cui's group [132] reported the synthesis of an S and N co-doped HPC composite (SN@LC) using lignite as the C precursor. The obtained material exhibits a well-developed porous structure. BET analysis revealed that $SN_{1/5}$@LC possesses a significantly higher SSA (246.64 m^2 g^{-1}) compared to pristine LC (46.10 m^2 g^{-1}), along with a micro-/meso-porous network that promotes electrolyte penetration and ion transport. Benefiting from the combined effects of increased SSA and S/N co-doping, the SN@LC electrode demonstrates enhanced electrochemical performance, delivering a reversible capacity of 347.5 mAh g^{-1} after 100 cycles at 0.1 A g^{-1} with 94% capacity retention.

Likewise, Zhou et al. [133] reported the synthesis of a sponge-like C material with hierarchical porosity derived from recycled laboratory coats (Figure 12b). The resulting NS-C-1100 anode exhibits excellent electrochemical performance, delivering a capacity of 313.5 mAh g^{-1} at 1 A g^{-1} and retaining 250 mAh g^{-1} over 7000 cycles, indicating outstanding cycling stability. Mechanistic studies attribute the enhanced performance to the cooperative interactions of heteroatom doping, expanded interlayer spacing, and a defect-rich C framework. Furthermore, DFT calculations combined with machine learning simulations reveal that vacancy defects and N/S dopants significantly enhance K-ion adsorption and storage behavior. When assembled into a full cell with a Prussian blue (PB) cathode, the NS-C-1100 anode maintains stable cycling for over 200 cycles at 1 A g^{-1} (Figure 12c), highlighting its practical application potential. This defect-engineering strategy offers a promising pathway for advanced K-storage.

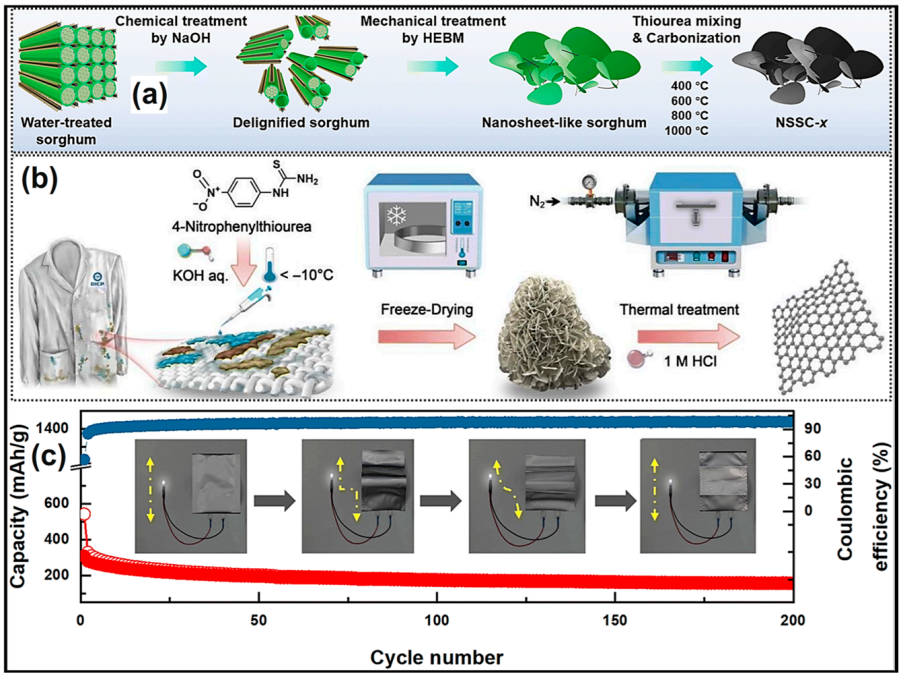

Figure 12. (**a**) Schematic illustration of synthesis pathway for NSSC-*x*. Adapted [131]. Copyright 2023, Royal Society of Chemistry. (**b**) Schematic representation of fabrication activity of NS-C-1100. (**c**) Cycling capability of NS-C-1100 electrode. Adapted [133]. Copyright 2023, Royal Society of Chemistry.

4.2.6. N and Se Co-Doping

The limited electron delocalization of pyrrolic N within five-membered rings causes pronounced polarization of neighboring N-C bonds, which slows K-ion extraction kinetics and results in irreversible capacity loss. Although introducing P or S to partially replace pyrrolic N can improve K-ion transport, it simultaneously reduces the overall N content. This trade-off remains a key challenge in tuning K-ion adsorption/desorption behavior at pyrrolic-N sites in HC, thereby hindering highly reversible electrochemical performance.

To overcome this limitation, Xu and co-workers [134] designed Se/N incorporated hard CNTs (h-CNTs) enriched with N-Se-C covalent linkages, which generate distinct localized electronic structures (Figure 13a). The incorporation of heteroatoms with markedly different electronegativities adjacent to N sites enables redistribution of the polarized electron density. Benefiting from its relatively low electronegativity and robust electron-donating capability associated with d-orbital participation [135], Se effectively compensates the charge imbalance among C and N (Figure 13b). Consequently, Se donation weakens the excessively strong interaction between K^+ ions and electronegative N sites, promoting more facile K^+ release during discharge and thereby improving electrochemical reversibility while suppressing capacity decay. DFT results further revealed that N incorporation markedly enhances K^+ adsorption compared with pristine C, with the E_{ads} decreasing from -0.48 to -1.03 eV (Figure 13c). Notably, simultaneous N and Se incorporation further strengthened K^+ adsorption, resulting in E_{ads} of -1.68 eV and signifying a substantial improvement in K^+ storage capability. This enhancement originates from electron donation by Se d orbitals, which alleviates polarization of pyrrolic N-C bonds and introduces mobile charge carriers that help balance the adsorption–desorption equilibrium of K^+ ions (Figure 13d). When assembled into binder-free anodes with mass loadings ranging from 1.5 to 2.4 mg cm^{-2}, the material demonstrated outstanding electrochemical performance, delivering a gravimetric capacity of 341 mAh g^{-1} at 0.2 A g^{-1} and achieving areal capacities as high as 4.06 mAh cm^{-2}. In addition, a capacity of 209 mAh g^{-1} was preserved at 8 A g^{-1} (93.3% retention), together with stable cycling after 2000 cycles while maintaining a stable Se/N ratio.

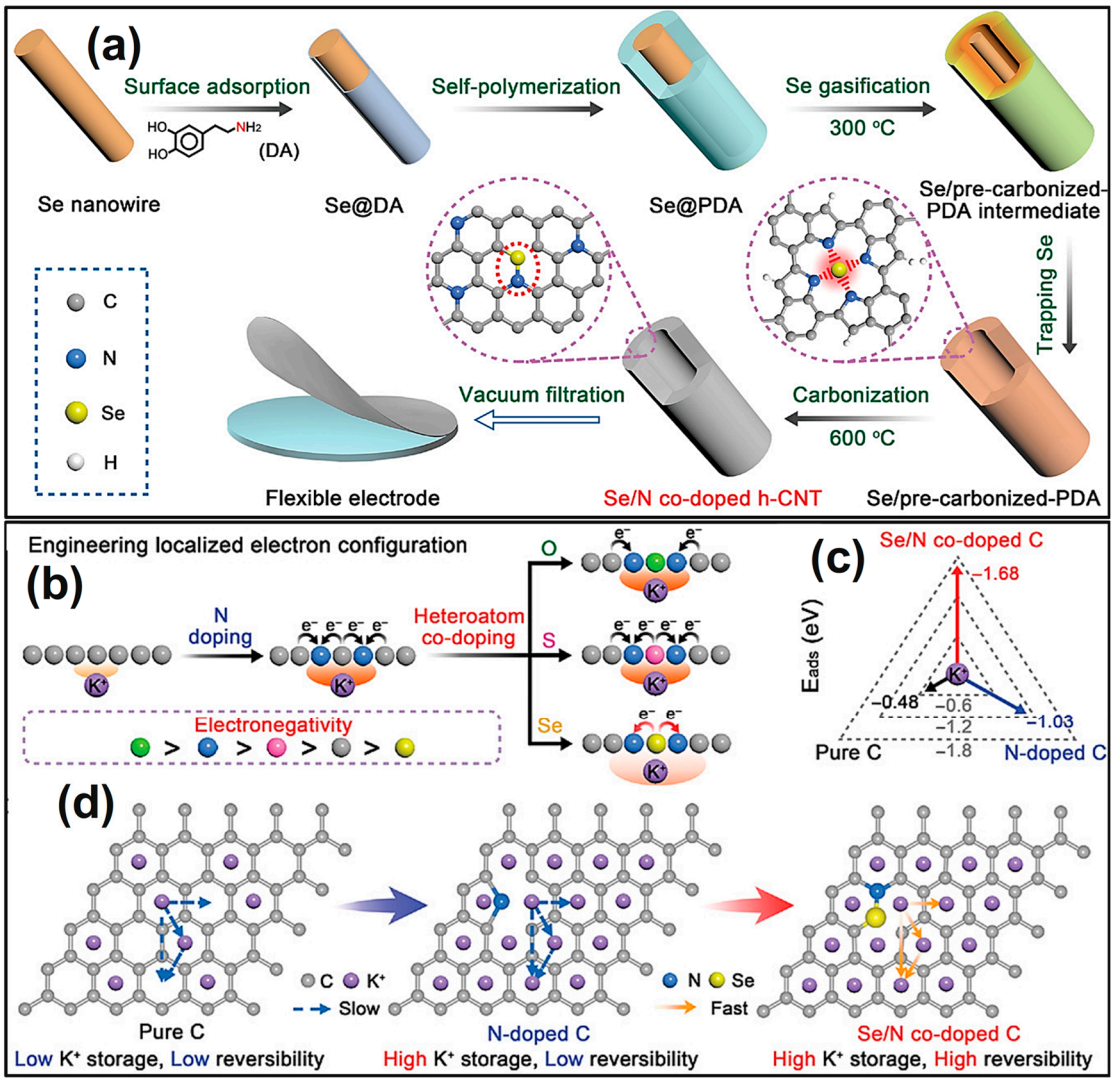

Figure 13. (**a**) Schematic representation of fabrication strategy for a binder-free Se/N incorporated h-CNT film. (**b**) Pictorial demonstration of charge redistribution in doped C frameworks arising from electronegativity differences. (**c**) DFT-derived adsorption energies of K^+ ions. (**d**) Proposed pathways for K^+ storage and diffusion. Adapted [134]. Copyright 2023, Wiley.

4.2.7. N and I Co-Doping

Due to their relatively large atomic radius (~140 pm), iodine (I) atoms tend to localize at the surfaces or edges of C materials rather than integrating into the bulk lattice [136]. This non-uniform distribution poses challenges for achieving homogeneous modification within the C framework, thereby increasing the complexity of synthesis. However, this characteristic can be deliberately exploited to improve electrochemical performance.

Chen's team [137] reported the synthesis of an I/N co-doped hierarchical C (I/N-HC) via an HF-assisted solvothermal strategy, using glucose as the C precursor and NH_4I as a dual-source dopant for both N and I. This co-doping strategy offers two primary benefits: it modulates the electronic structure of the C framework to create additional K-ion active sites, and theoretical calculations indicate that I incorporation effectively enlarges the interlayer spacing. Consequently, the combined effects of lattice expansion and strengthened K-C interactions markedly enhance K-ion adsorption. Electrochemical tests show that the I/N-HC electrode maintains a reversible capacity of ~149 mAh g^{-1} after 400 cycles at 0.5 A g^{-1}. DFT calculations further demonstrate a strong synergistic interaction between I and N dopants, with Eads decreasing from −1.33 eV for pristine

C to −3.27/−3.63 eV for I-doped C and −3.71 eV for N-C, ultimately reaching −4 eV in the co-doped system. In combination with polyiodide-mediated charge transport and I-induced interlayer expansion, the optimized electronic structure introduces more active sites and promotes rapid K-ion diffusion, thereby leading to improved PIB performance. This study underscores the importance of I/N co-doping and offers valuable guidance for the rational design of HC-based electrodes.

4.2.8. O and F Co-Doping

Fluorine (F), the most electronegative element, readily forms covalent C-F bonds with graphitic C, inducing a partial transition in C hybridization from sp^2 to sp^3 [138]. The inherently narrow interlayer spacing of graphite (3.35 Å) significantly restricts K-ion intercalation. Incorporation of F effectively modulates the interlayer distance, thereby facilitating K-ion insertion [121]. In addition, strong F-C interactions improve electronic conductivity and lower the energy barriers for K-ion adsorption and diffusion, leading to enhanced rate performance.

Wine lees have recently been explored as a sustainable biomass precursor for fabricating F/O co-doped HCs (FO-HCs). By tuning the carbonization temperature, flexible C sheets with optimized morphology and well-defined pore structures were achieved [139]. The hierarchical porosity enhances electrolyte accessibility and provides abundant pathways for ion transport and K-ion storage, leading to improved electrochemical performance. Depth-profile XPS confirms uniform F distribution, with consistent concentrations at etching depths of 15 and 30 nm, indicating successful bulk doping. K 2p spectra reveal interactions between K and both C and F species, suggesting that F-related defects serve as dominant K-ion storage sites. DFT calculations demonstrate that F/O co-doping regulates K-ion adsorption behavior; specifically, F-C shows an Eads of −2.183 eV, compared to −1.788 eV for pristine C and −2.3 eV for O-C, indicating a balanced adsorption strength. Charge density analysis further confirms electron transfer from K to doped sites, reinforcing binding and structural integrity. Combined DFT and in situ XPS results indicate that F doping optimizes K-ion adsorption strength, mitigates capacity fading, and accelerates charge transfer. As a PIB anode, FO-HC1200 achieves a high capacity of 409.1 mAh g^{-1} at 0.1 A g^{-1}. In situ Raman and XRD analyses reveal a dual storage mechanism involving surface adsorption at high potentials and intercalation at low potentials. These results guide the design of high-performance HC anodes.

4.2.9. O and S Co-Doping

The design of amorphous, heteroatom-doped, and highly porous C nanostructures plays a vital role in improving PIB performance [140]. Yang's team [140] developed a carbonization-etching approach to synthesize S/O co-doped porous C microspheres (PCMs) using polymer-derived templates (Figure 14a). The resulting materials exhibit an ordered porous network, high SSA, enlarged interlayer spacing, and abundant structural defects characteristic of amorphous C. These features collectively facilitate K-ion storage, enabling capacities of 226.6 mAh g^{-1} at 0.05 A g^{-1} over 100 cycles and 108.4 mAh g^{-1} after 2000 cycles at 1 A g^{-1}. DFT calculations reveal that S/O doping enhances K-ion adsorption and alleviates structural distortion during cycling. This study highlights the synergistic role of hierarchical porosity and heteroatom incorporation in optimizing K-storage.

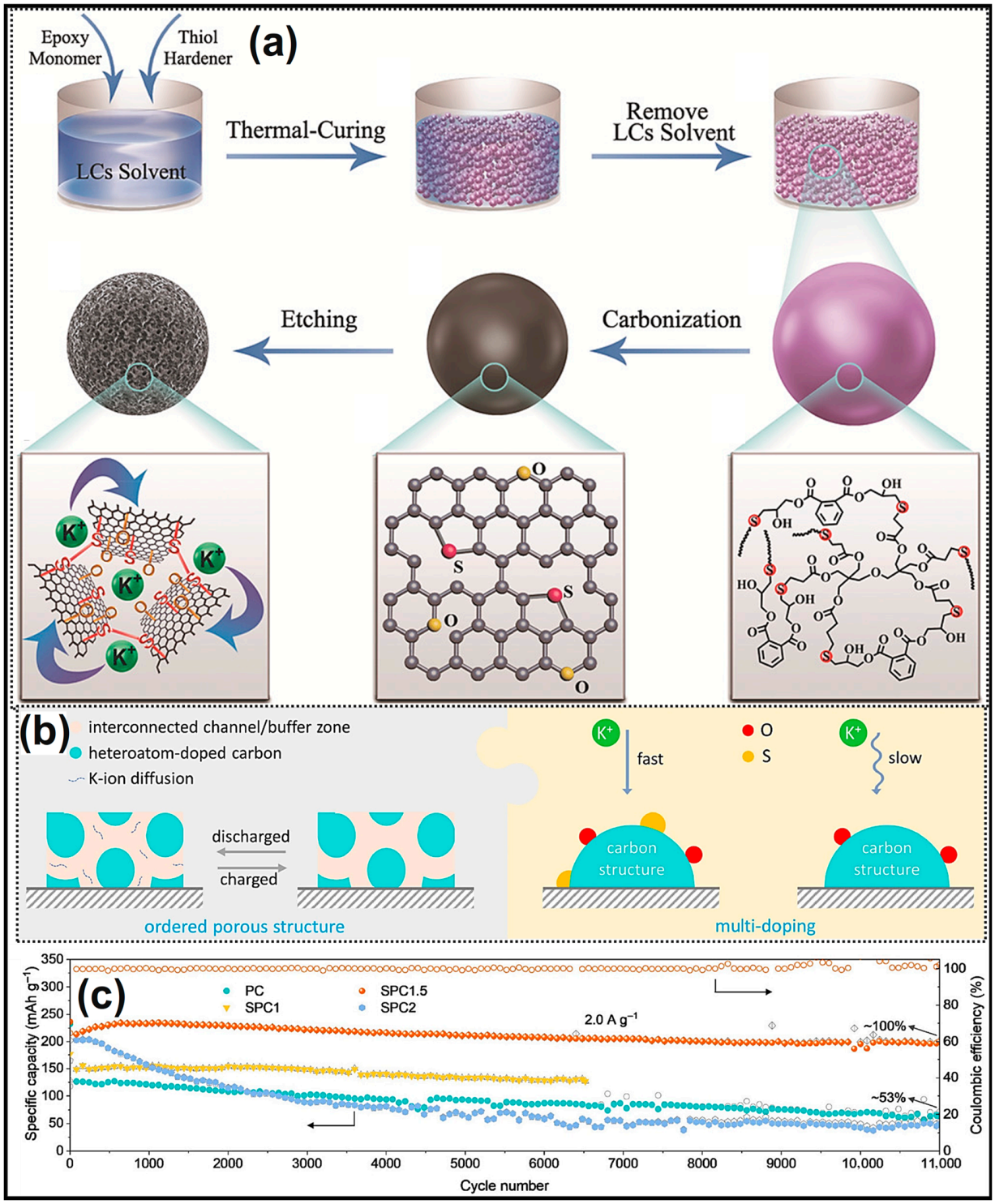

Figure 14. (**a**) Schematic representation of the PCM preparation pathway. Adapted [140]. Copyright 2018, Wiley. (**b**) Illustration of pore expansion and improved K^+ adsorption induced by multi-heteroatom doping. (**c**) Cycling behavior. Adapted [141]. Copyright 2024, American Chemical Society.

Yang and co-workers [141] reported the fabrication of O/S co-doped HC (SPC) with a highly ordered porous architecture for long-life PIB applications. Elemental line-scanning analysis confirmed the uniform distribution of C, S, and O throughout the microspheres without phase separation, indicating that heteroatoms are chemically integrated into the C framework. Both experimental results and DFT calculations demonstrate that this structure

facilitates rapid K-ion diffusion and reversible insertion/extraction, enhances electrolyte accessibility, and provides abundant active sites, thereby improving redox kinetics and cycling stability (Figure 14b). Consequently, the SPC electrode delivers 200 mAh g^{-1} at 2 A g^{-1} and maintains nearly 100% capacity retention over 11,000 cycles (Figure 14c), surpassing most reported C-based electrodes. These results offer important insights for designing durable PIB anodes.

4.3. Ternary Doping

Ternary heteroatom doping in HC has attracted growing interest as an effective strategy for improving PIB performance [142]. Introducing three different dopants simultaneously can generate strong cooperative interactions that enhance both reversible capacity and cycling stability. The presence of multiple heteroatoms forms a highly functionalized and structurally complex C framework, which increases electrochemical activity, provides numerous K-ion storage sites, and improves electronic conductivity. Such multi-element doping promotes rapid ion transport and stabilizes the structure during long-term cycling, thereby mitigating capacity fading. Overall, the cooperative interactions among various heteroatoms make ternary-doped HC a promising candidate for advanced energy storage systems.

4.3.1. N, P, and S Co-Doping

Biomass-derived HCs generally retain the morphology of their precursors and often exhibit limited porosity, which can hinder ion transport and increase electrochemical polarization. To overcome these limitations, heteroatom-doped HCs with engineered hierarchical structures have been developed as promising anode materials for PIBs. Li and co-workers [143] developed a biomass-derived strategy to synthesize multi-heteroatom doped C spheres (NPS-FCMs), mainly doped with N and containing minor amounts of P and S (Figure 15a). This approach enables high doping levels while constructing a highly disordered, hierarchically porous structure. Compared to C spheres obtained from a single precursor such as glucose, NPS-FCM exhibits improved initial Coulombic efficiency (ICE), rate performance, and cycling stability. As a result, the assembled NPS-FCM//PTCDA full cell operates at 1.78 V and demonstrates excellent long-term cycling stability (Figure 15b,c), indicating strong practical potential. In situ Raman analysis, combined with electrochemical measurements, reveals a hybrid K-ion storage mechanism involving adsorption/desorption, alloying-like potassiation/depotassiation, and pore filling (Figure 15d). DFT calculations further confirm enhanced electrical conductivity and reduced K-ion E_{ads} in NPS-FCM. These results highlight that mixed-biomass synthesis enables synergistic structural regulation and in situ multi-heteroatom doping, providing an effective strategy for advanced electrode design.

4.3.2. N, O, and P Co-Doping

Many biomass precursors inherently possess well-defined and complex biological structures, making them attractive templates for designing PIB anodes [144]. In particular, HCs co-doped with three heteroatoms derived from plant or animal sources have been shown to enhance both ionic and electronic interactions at dopant-rich sites. For example, an N/O/P co-doped C sphere (NOP-PB), synthesized using sessile puffball as a template, has been successfully applied as a PIB electrode [145]. XPS analysis was employed to examine the chemical bonding states of the incorporated heteroatoms (N, O, and P). Deconvolution of the N 1s spectrum reveals four N configurations: pyridinic-N (398.44 eV), pyrrolic-N (400.5 eV), graphitic-N (401.14 eV), and oxidized N-O (402.8 eV). Meanwhile, the P 2p spectrum shows characteristic peaks corresponding to P-C (132.7 eV), P-O/P-O-C (134.2 eV), and P-N (135.5 eV), confirming successful incorporation of N and P

into the C framework. XRD results indicate a shift in the (002) peak toward lower angles relative to graphite, suggesting an increased interlayer spacing from 3.356 to 3.721 Å for NOP-PB-2, as calculated by Bragg's law. This enlarged spacing facilitates reversible K-ion insertion and extraction. Electrochemical testing indicates that NOP-PB with optimized heteroatom composition exhibits excellent rate capability and long-term cycling performance. The electrode delivers capacities of 352.2 mAh g^{-1} after 200 cycles at 0.2 A g^{-1} and 303.5 mAh g^{-1} after 2000 cycles at 0.5 A g^{-1}. Even at high current densities of 2–5 A g^{-1}, it maintains 242.4 mAh g^{-1} over 1300 cycles and 160.3 mAh g^{-1} over 2000 cycles. These results highlight the combined effects of expanded interlayer spacing, ternary heteroatom doping, and a hierarchical porous hollow-sphere structure in enhancing electrochemical performance. Derived from sustainable sessile puffballs and possessing favorable structural features, this material shows strong potential for scalable PIB anodes.

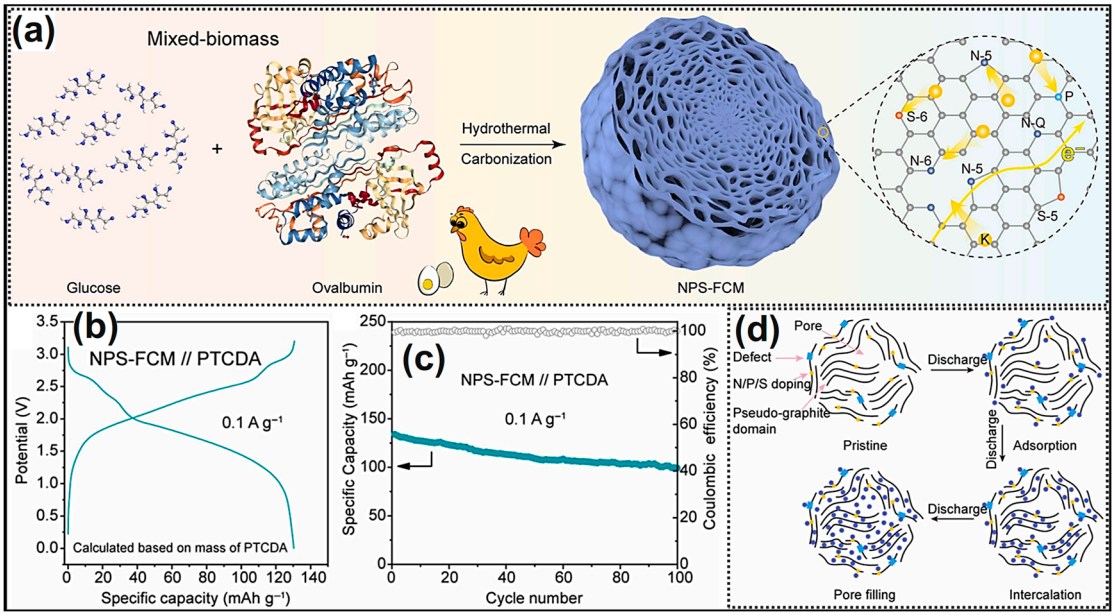

Figure 15. (**a**) Schematic representation of synthesis route for NPS-FCM. (**b**) Galvanostatic charge–discharge curves. (**c**) Cycling behavior. (**d**) Schematic illustration of the K^+ storage process. Adapted [143]. Copyright 2023, Elsevier.

4.3.3. N, O, and S Co-Doping

Introducing heteroatoms into C frameworks through covalent bonding significantly increases the density of electrochemically active sites, leading to enhanced performance via alterations in electronic structure and surface chemistry [146]. While N doping alone mainly enhances adsorption due to its strong electron-withdrawing nature, the simultaneous incorporation of multiple heteroatoms produces synergistic interactions that markedly improve reaction kinetics. Based on this strategy, N, O, and S tri-doped HC (NOS-HC) spheres were fabricated through a simple one-step annealing process using waste tires as a precursor [147]. During pyrolysis, the tire material converts into a heteroatom-enriched C network, where S originates from C-S bonds in rubber, and N and O are supplied by additives, forming functional groups such as C-S-C, pyridinic N, and C-O species. Among the prepared samples, NOS-HC900 exhibits a hierarchical porous structure with graphitic, vortex-like C layers. CV analysis indicates that charge storage is predominantly governed by surface-controlled capacitive processes, resulting in superior rate capability and long-term cycling stability due to rapid charge-transfer kinetics. These improvements arise from the combined effects of multi-heteroatom doping and a

well-developed micro-/meso-porous structure, which together enhance ion diffusion and charge storage.

The synergistic effect of N, O, and S co-doping in C materials arises from their distinct yet complementary roles in modulating K-ion adsorption. N and O, due to their high electronegativity, create strong adsorption sites that contribute to increased capacity, whereas S, with its larger atomic size and relatively weaker electronic influence, helps prevent excessively strong K-ion binding. This optimized adsorption balance ensures reversible ion insertion and extraction. Moreover, the combined presence of multiple heteroatoms promotes charge redistribution and enhances electrical conductivity, thereby improving overall electrochemical performance. During K-ion storage, ions initially adsorb onto defect-rich edge sites and subsequently intercalate into expanded C layers via quasi-ionic interactions characterized by relatively low binding energies. Importantly, S acts as a modulator by weakening the strong adsorption induced by N and O, facilitating the diffusion of solvated K-ions across the surface. This regulated interaction enables a dual storage mechanism involving both surface adsorption and vacancy-assisted insertion. Consequently, NOS-HC900 achieves an initial capacity of 342.6 mAh g^{-1} at 0.1 A g^{-1}, a reversible capacity of 322.7 mAh g^{-1}, and retains 231.7 mAh g^{-1} at 2 A g^{-1}.

A novel HC anode (NOSHC) for PIBs was fabricated using a simple low-temperature thermal decomposition approach. The mild treatment conditions effectively preserve structural defects, thereby creating abundant active sites for K-ion storage. Systematic investigation of synthesis parameters indicates that lower carbonization temperatures help retain a high density of defects, which enhances adsorption capacity, while the lamellar structure shortens ion diffusion pathways and facilitates transport kinetics. Furthermore, an appropriate level of porosity suppresses undesirable side reactions. Among the obtained samples, NOSHC-101-500-1 exhibits a slope-dominated voltage profile and delivers outstanding electrochemical performance, retaining approximately 50% of its reversible capacity at 5 A g^{-1}. During prolonged cycling, the electrode undergoes continuous electrochemical activation through repeated potassiation and depotassiation processes, leading to reduced polarization, decreased R_{ct}, and a gradual increase in capacity after the initial decay, ultimately reaching 210 mAh g^{-1} after 1000 cycles. Ex situ Raman analysis confirms this activation behavior, revealing a progressive increase in defect density upon cycling.

4.3.4. N, S, and Se Co-Doping

The simultaneous incorporation of N, S, and Se into HC introduces abundant structural defects and electrochemically active pathways, thereby enhancing electrical conductivity and facilitating ion transport for improved K-storage. Wu's group [148] reported the synthesis of N, S, and Se co-doped HC (SSHC) via a scalable method using PAN and Se sulfide as precursors. When evaluated as an anode for PIBs, SSHC delivered a capacity of 207 mAh g^{-1} after 450 cycles at 0.1 A g^{-1} and retained 143.5 mAh g^{-1} after 1100 cycles at 1 A g^{-1}. Additionally, a capacity of 158.1 mAh g^{-1} was achieved at a high current density of 3 A g^{-1}, indicating excellent rate capability. Kinetic studies reveal that the improved performance arises from enhanced capacitive contributions and increased ion diffusion coefficients, attributed to the combined effects of hierarchical structure and multi-heteroatom doping. The straightforward synthesis combined with superior electrochemical performance highlights SSHC as a promising candidate for energy storage and electrocatalytic applications.

To evaluate the impact of different non-metal heteroatoms on PIB performance, Table 1 compiles key metrics including ICE, cycling stability, and rate capability for the previously discussed heteroatom-doped HCs. Comparative analysis indicates that N and B co-doped

Ni@BNHC delivers an exceptionally high capacity of 631 mAh g^{-1}. Meanwhile, N-doped MCS and multi-heteroatom modified O-NCNFs (N, O, and S) exhibit relatively high ICE values exceeding 77%, underscoring the beneficial role of heteroatom incorporation in promoting stable SEI formation. Superior rate performance is observed in N,O-doped NOBC, which achieves 222.6 mAh g^{-1} at 2 A g^{-1}, and in N,S,Se-doped h-CNTs, which maintain 224 mAh g^{-1} at 8 A g^{-1}, highlighting the synergistic advantages of multi-heteroatom doping under high current densities. Excellent long-term stability is demonstrated by N,F-doped CDC-F-900, retaining 214.2 mAh g^{-1} after 5000 cycles, and N,S-doped NS-C, sustaining 250 mAh g^{-1} over 7000 cycles, suggesting that F and S play crucial roles in enhancing structural integrity during extended cycling. In contrast, materials with extremely high reversible capacities, such as S-HMCNS (599.5 mAh g^{-1}), often exhibit low ICE values (36%), indicating a trade-off between capacity and initial efficiency. Overall, co-doping strategies involving N/B and N/O/S provide a more balanced optimization of capacity and stability, although further improvements are required to simultaneously achieve high-rate performance and ICE.

Table 1. Electrochemical behavior comparison of HC anodes with different heteroatom doping strategies.

Doping	Sample	Electrolyte [Voltage Window]	Reversible Capacity (mAh g^{-1}) [Current Density (A g^{-1})]	ICE (%)	Rate Performance (mAh g^{-1}) [Current Density (A g^{-1})]	Cycle Performance (mAh g^{-1}) [Cycle Number, Current Density (A g^{-1})]	Ref.
B	BZPC	0.8 M KPF_6/ethylene carbonate (EC)/diethyl carbonate (DEC) (1:1 volume ratio) [0.01–3 V]	223.8 [0.05]	31.76	130.9 [1.0]	115.9 [2000, 1.0]	[61]
N	NCS	0.8 M KPF_6 in a mixture of EC and DEC (1:1 by volume) [0.01–3 V]	250 [0.033]	46.7	154 [20.160]	180 [4000, 0.504]	[68]
N	N-SPC	0.8 M KPF_6 in a mixture of EC and DEC (1:1 by volume) [0.01–3 V]	329 [0.1]	40	116 [20.0]	296 [2000, 1.0]	[69]
N	NPC	0.8 M KPF_6 in a mixture of EC and DEC (1:1 by volume) [0.01–3 V]	419.7 [0.05]	43.1	185 [10.0]	226.1 [1000, 1.0]	[70]
N	NGHCs	0.8 M KPF_6 in a mixture of EC and DEC (1:1 by volume) [0.01–3 V]	298.8 [0.05]	34.84	132.2 [1.0]	137.6 [1000, 0.5]	[78]
N	NHC	0.8 M KPF_6 in a mixture of EC and DEC (1:1 by volume) [0.01–2.5 V]	402 [0.05]	76	263 [0.2]	176 [260, 1.0]	[79]
N	MCS	0.8 M KPF_6 in a mixture of EC and DEC (1:1 by volume) [0.01–3 V]	351.4 [0.05]	78.81	107.9 [5.0]	113.9 [3600, 1.0]	[73]
N	NMCNFs	1.0 M KPF_6 in a mixture of EC and DEC (1:1 by volume) [0.01–3 V]	351.1 [0.2]	44.7	134 [10.0]	122.3 [20,000, 5.0]	[75]
N	N-CNFs	0.8 M KPF_6 in a mixture of EC and DEC (1:1 by volume) [0.01–3 V]	332 [0.1]	41.3	144 [5.0]	195 [2000, 1.0]	[149]
N	LCN	1.0 M KPF_6 in a mixture of EC and DEC (1:1 by volume) [0.01–3 V]	314 [0.1]	41.53	152.6 [1.0]	124.3 [1500, 1.0]	[150]
O	P-HC	3 M Potassium bis(fluorosulfonyl)imide (KFSI) in monoglyme (DME) [0.01–3 V]	352.8 [0.1]	26.8	154.4 [1.0]	151.9 [2500, 1.0]	[82]
O	VCA	0.8 M KPF_6 in a mixture of EC and DEC (1:1 by volume) [0.01–2.5 V]	258 [0.0279]	34	148 [0.458]	151 [1000, 0.0279]	[83]
P	PHC-700	0.8 M KPF_6 in a mixture of EC and DEC (1:1 by volume) [0.01–3.0 V]	381.9 [0.1]	45.7	224 [1.0]	260 [1000, 0.2]	[84]
P	HC-1300-P	0.8 M KPF_6 in a mixture of EC and DEC (1:1 by volume) [0.005–2.5 V]	302 [0.05]	46	138 [1.0]	175 [700, 0.3]	[85]
S	S-HC	1.0 M KFSI in DME [0.001–2.0 V]	270 [0.2]	43.1	196 [1.0]	191 [300, 1.0]	[151]
S	SDHC	0.8 M KPF_6 in a mixture of EC and DEC (1:1 by volume) [0.01–2.5 V]	416 [0.05]	45	286 [1.0]	190 [450, 1.0]	[152]
S	SHPCS	0.8 M KPF_6 in 4:3:2 (volume ratio) Ethylene Carbonate (EC): Dimethyl Carbonate (DMC): Ethyl Methyl Carbonate (EMC) [0.01–3.0 V]	454 [0.05]	64.9	219 [1.0]	211.4 [1000, 1.0]	[91]
S	HS-HC	0.8 M KPF_6 in a mixture of EC and DEC (1:1 by volume) [0.01–2.5 V]	317.7 [0.05]	36.05	161 [0.8]	219.2 [240, 0.1]	[153]

Table 1. *Cont.*

Doping	Sample	Electrolyte [Voltage Window]	Reversible Capacity (mAh g^{-1}) [Current Density (A g^{-1})]	ICE (%)	Rate Performance (mAh g^{-1}) [Current Density (A g^{-1})]	Cycle Performance (mAh g^{-1}) [Cycle Number, Current Density (A g^{-1})]	Ref.
S	SHC-3	1 mol L^{-1} KFSI into the solvent of EMC [0.01–3.0 V]	362.2 [0.05]	51.3	119.5 [1.0]	220.2 [5200, 0.5]	[93]
S	SC-700	0.8 M KPF_6 in a mixture of EC and DEC (1:1 by volume) [0.01–3.0 V]	442 [0.05]	42	288 [1.0]	250.5 [1000, 1.0]	[94]
S	SCNs	1.0 M KPF_6 in a mixture of EC and DEC (1:1 by volume) [0.005–3.0 V]	300 [0.05]	55.9	85 [1.0]	81 [1000, 1.0]	[99]
S	MCSs	0.8 M KPF_6 in a mixture of EC and DEC (1:1 by volume) [0.01–3.0 V]	325 [0.1]	43.4	144 [5.0]	180 [1000, 1.0]	[100]
S	S-HMCNS	1.0 M KFSI solution dissolved in DME [0.01–3.0 V]	599.5 [0.05]	36	216.6 [1.0]	197 [1400, 2.0]	[101]
S	SHC	0.8 M KPF_6 in a mixture of EC and DEC (1:1 by volume) [0.01–2.5 V]	405.2 [0.05]	48.2	264 [1.0]	128.2 [1500, 2.0]	[95]
N/B	NBPC2	1 M KFSI solution in a 1:1 (v/v) mixture of EC and DMC [0.01–3.0 V]	534 [0.1]	40.5	294.7 [1.0]	358.9 [3000, 2.0]	[107]
N/B	Ni@BNHC	0.85 M KPF_6 in a mixture of EC and DEC (1:1 by volume) [0.01–3.0 V]	631 [0.05]	32.8	268 [1.0]	259 [1500, 1.0]	[108]
N/O	MCOs	1.0 M KPF_6 in a mixture of EC and DEC (1:1 by volume) [0.01–3.0 V]	364 [0.05]	65.7	110 [1.0]	80 [3000, 2.0]	[115]
N/O	NOHPHC	1.0 M KPF_6 in a mixture of EC and DMC (1:1 by volume) [0.001–3.0 V]	315 [0.05]	45.4	150 [1.0]	130 [1100, 1.05]	[116]
N/O	NO-HC	3 M KFSI solution in DME [0.01–3.0 V]	342 [0.1]	49.3	264.5 [1.0]	235 [1200, 2.0]	[117]
N/O	NOHC	0.8 M KPF_6 in a mixture of EC and DMC (1:1 by volume) [0.01–3.0 V]	304.6 [0.1]	50.7	254.4 [1.0]	189.5 [5000, 1.0]	[120]
N/O	NOBC	1.0 M KPF_6 dissolved in EC/DEC (volume ratio 1:1) [0.01–3.0 V]	251.2 [0.5]	64.3	222.6 [2.0]	334.6 [2000, 5.0]	[118]
N/O	NOCNBs	0.8 M KPF_6 dissolved in EC/DEC (volume ratio 1:1) [0.01–3.0 V]	468 [0.05]	49	286 [0.8]	277 [1600, 1.0]	[154]
N/O	NO-YS-CS	1 M KPF_6 in the mixture of EC, DEC, and PC with the volume ratio of 1:1:1 [0.01–2.0 V]	391.5 [0.05]	31	183.8 [1.0]	189.2 [2500, 0.5]	[155]
N/F	CDC-F-900	1.0 M KPF_6 dissolved in EC, DEC and EMC (volume ratio 1:1:1) with 5.0% FEC [0.01–2.9 V]	516.9 [0.1]	55.4	385.4 [1.0]	214.2 [5000, 10.0]	[121]
N/P	PN-PCM	0.8 M KPF_6 dissolved in EC/DEC (volume ratio 1:1) [0.01–3.0 V]	453 [0.05]	63.6	168 [5.0]	218 [3000, 1.0]	[123]
N/P	N/P-HPCB	1 M KFSI solution in DME [0.01–3.0 V]	525.3 [0.05]	58.3	213.6 [4.0]	205.2 [1000, 2.0]	[124]
N/P	HCNS-NP	0.8 M KPF_6 dissolved in EC/DMC (volume ratio 1:1) [0.01–3.0 V]	338.8 [0.1]	49.8	116.4 [2.0]	180.6 [1000, 1.0]	[125]
N/P	PNHC	0.8 M KPF_6 dissolved in EC/DMC (volume ratio 1:1) [0.01–3.0 V]	535.9 [0.05]	56.9	268.1 [1.0]	270.4 [1000, 1.0]	[128]
N/P	N/P-HPCS	0.8 M KPF_6 dissolved in EC/DEC (volume ratio 1:1) [0.01–3.0 V]	453.4 [0.2]	20	193 [0.4]	137.6 [1500, 2.0]	[126]
N/P	NPDCs	0.8 M KPF_6 dissolved in EC/DEC (volume ratio 1:1) [0.01–3.0 V]	420 [0.1]	44	280 [1.0]	138 [2000, 2.0]	[156]
N/P	NPHC	0.8 M KPF_6 dissolved in EC/DEC (volume ratio 1:1) [0.01–3.0 V]	253 [0.1]	58.8	174 [1.0]	172 [1000, 2.0]	[157]
N/S	HS	1 M KPF_6 which was dissolved in DMC, ethyl methyl carbonate (EMC) and EC in a volume ratio of 1:1:1 [0.01–3.0 V]	362 [0.1]	50	190 [1.0]	148 [1000, 1.0]	[129]
N/S	SNHC	1.0 M KPF_6 dissolved in EC/DEC (volume ratio 1:1) [0.01–3.0 V]	213.7 [0.1]	35.2	199 [1.5]	144.9 [1200, 3.0]	[158]
N/S	NSPC	0.8 M KPF_6 dissolved in EC/DEC (volume ratio 1:1) [0.01–3.0 V]	285.3 [0.05]	68.8	150 [1.0]	125.5 [1000, 1.0]	[159]
N/S	NSSC	1 M potassium bis(fluorosulfonyl)imide in a mixed solvent of EC/PC (volume ratio of 1:1) [0.01–3.0 V]	268 [0.1]	60	131 [1.0]	110 [2400, 1.0]	[131]
N/S	SN@LC	1.0 M KPF_6 dissolved in EC/DEC (volume ratio 1:1) [0.01–3.0 V]	347.5 [0.1]	54.7	185.5 [1.0]	136 [1500, 1.0]	[132]
N/S	NS-C	0.8 M KPF_6 dissolved in EC/DEC (volume ratio 1:1) [0.01–3.0 V]	583 [0.1]	58.6	313.5 [1.0]	250 [7000, 1.0]	[133]

Table 1. *Cont.*

Doping	Sample	Electrolyte [Voltage Window]	Reversible Capacity (mAh g^{-1}) [Current Density (A g^{-1})]	ICE (%)	Rate Performance (mAh g^{-1}) [Current Density (A g^{-1})]	Cycle Performance (mAh g^{-1}) [Cycle Number, Current Density (A g^{-1})]	Ref.
N/Se	h-CNTs	1.0 M KFSI dissolved in EC/DEC (volume ratio 1:1) [0.01–3.0 V]	345 [0.2]	51.8	224 [8.0]	209 [2000, 8.0]	[134]
N/P/S	NPS-FCM	0.8 M KPF_6 dissolved in EC/DEC (volume ratio 1:1) [0.01–3.0 V]	257.9 [0.05]	56.1	179.4 [1.0]	162.1 [1000, 1.0]	[143]
N/O/P	NOP-PB	1.0 M KPF_6 dissolved in EC/DEC (volume ratio 1:1) [0.01–3.0 V]	352.2 [0.2]	31.7	274.8 [1.0]	160.3 [2000, 5.0]	[145]
N/O/S	NOS-HCs	1.0 M KPF_6 in a mixed solution of EC, DEC, and EMC (1:1:1 in Vol) with 0.5% FEC [0.01–2.9 V]	323.1 [0.1]	38	252.3 [1.0]	322.7 [1000, 0.1]	[147]
N/O/S	NOSHC	1.0 M KFSI dissolved in EC/DEC (volume ratio 1:1) [0.01–3.0 V]	265 [0.1]	51	125 [5.0]	210 [1000, 1.0]	[142]
N/O/S	O-NCNFs	1.0 M KPF_6 dissolved in EC/DEC (volume ratio 1:1) [0.01–3.0 V]	423 [0.05]	77.5	251 [1.0]	362 [300, 0.5]	[160]
N/O/S	SSHC	1.0 M KPF_6 dissolved in EC/DEC (volume ratio 1:1) [0.01–3.0 V]	252.5 [0.1]	34.9	187.9 [1.0]	143.5 [1100, 1.0]	[148]

Figure 16a illustrates a comparative evaluation of reversible capacity and ICE for electrodes modified via various doping strategies, including single-element doping (N, P, or S) and dual-element systems such as N/B and N/O, all tested under identical current density conditions. The results reveal a clear trade-off between achieving high capacity and maintaining acceptable ICE values. In particular, dual-doped materials (e.g., N/B and N/O) exhibit exceptionally high capacities exceeding 600 mAh g^{-1}; however, these improvements are accompanied by relatively low ICE values, typically ≤50%. In contrast, electrodes with single heteroatom doping (e.g., N or P) deliver moderate capacities in the range of 300–450 mAh g^{-1} while showing comparatively higher ICE. For more complex multi-element doping systems, such as N/P/S and N/O/S, the reversible capacity decreases to approximately 400–450 mAh g^{-1}, whereas ICE demonstrates a slight improvement relative to the high-capacity co-doped systems.

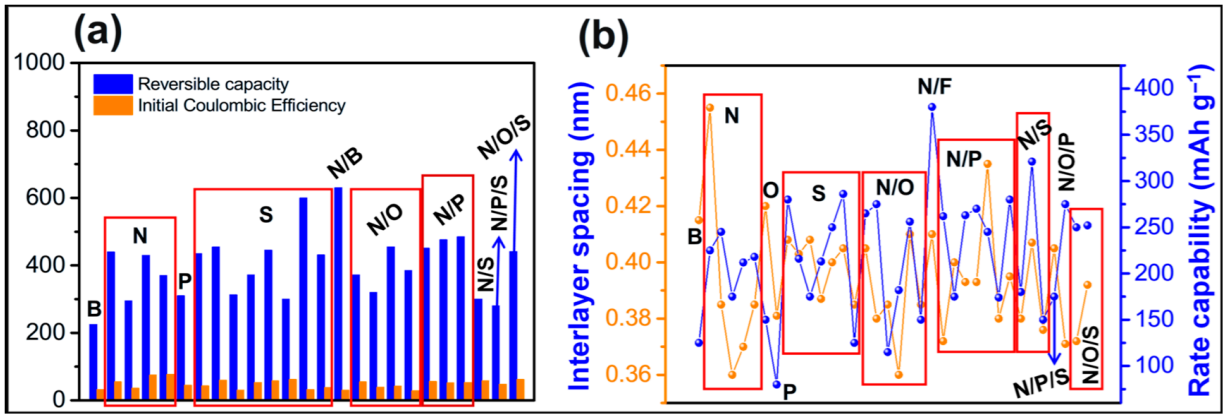

Figure 16. (**a**) Bar chart comparing capacity and ICE. (**b**) Relationship between rate performance and interlayer distance.

In general, increases in reversible capacity are often accompanied by a decline in ICE, indicating an inherent trade-off in performance. To overcome this limitation, the rational design of multi-heteroatom doping systems is crucial. Advanced modulation approaches, such as gradient dopant distribution and site-selective incorporation, can preserve the advantages of multiple active species while minimizing excessive interfacial side reactions caused by random doping. Furthermore, combining doping strategies

with structural engineering, such as the development of hierarchical porous networks or nanoscale architectures, can effectively shorten ion diffusion pathways, enhance electrode-electrolyte interactions, and reduce irreversible losses.

Figure 16b illustrates the correlation between interlayer spacing and rate performance for C materials modified via different heteroatom doping strategies. A generally positive relationship is observed, suggesting that increased interlayer distances facilitate enhanced high-rate capability. For S-doped carbons, the reversible capacity significantly increases from 119.5 mAh g^{-1} at 0.382 nm to 288 mAh g^{-1} at 0.41 nm. A similar trend is evident in N/S co-doped systems, where the capacity improves from 150 mAh g^{-1} at an interlayer spacing of 0.375 nm to 313.5 mAh g^{-1} at 0.406 nm. In singly doped materials, rate performance is largely dictated by the degree of interlayer expansion, as exemplified by P-doped C, which delivers only 92 mAh g^{-1} at 0.38 nm. In contrast, dual-doped systems exhibit pronounced cooperative interactions that enhance rate capability beyond the contribution of interlayer spacing alone. For instance, N/F co-doped C achieves 385.4 mAh g^{-1} at 0.41 nm, while certain N/O co-doped materials maintain strong rate performance even at relatively smaller interlayer distances. These results suggest that although interlayer expansion is a key structural parameter, co-doping introduces additional benefits that further improve high-rate electrochemical performance.

To elucidate the contributions of different incorporation strategies to performance enhancement and to offer design guidelines for doped HC electrodes, Table 2 provides a comprehensive summary of the functional roles, underlying mechanisms, structural features, and combined effects associated with single-, binary-, and ternary-heteroatom doping in PIB systems.

Table 2. Comparative summary of the functional effects and mechanisms of heteroatom doping in HC materials for PIB applications.

Doping	Core Principle	Key Characteristics	Main Effect	Trade-Offs/Limitations
N/S/Se	Mitigate N-C bond polarization and enhance electrochemical reversibility	N creates active sites, while S/Se modulate K^+ insertion and de-insertion	Improved reversible capacity and cycling stability via balanced adsorption/desorption	Possible structural disorder and reduced conductivity at high S/Se content; potential side reactions lowering ICE
N/O/P	Combine wettability, active sites, and structural stability	N and O enhance surface reactivity; P reinforces C framework	Enhanced rate capability and long-term stability due to improved electrolyte interaction and structural robustness	Excess O may cause unstable SEI; high P content may reduce conductivity or increase irreversible capacity
N/P/S	Synergistically enhance conductivity, active sites, and interlayer spacing	N improves conductivity; P stabilizes structure; S enlarges interlayer spacing	Simultaneous optimization of capacity, rate performance, and cycling durability	Increased synthesis complexity; excessive multi-doping may introduce inactive defects and lower ICE
N/O/S	Balance K^+ adsorption and diffusion kinetics	N/O enhance adsorption; S prevents overly strong binding	Fast ion transport with dual-mode (capacitive + diffusion) storage	Trade-off between capacity and ICE due to high defect density; possible structural instability at high doping levels
N/B	Optimize electronic structure via donor-acceptor interaction	N introduces defects; B shifts Fermi level	High conductivity and enhanced active site utilization → excellent rate capability	Imbalance in N/B ratio may reduce conductivity or create inactive sites; often lower ICE
N/P	Maximize active site exposure and structural integrity	N induces defects; P strengthens framework and expands spacing	High capacity with improved cycling stability due to strong K^+ adsorption	Excess P may distort structure and reduce conductivity; increased irreversible capacity
N/O	Combine conductivity with improved wettability	N enhances conductivity; O improves electrolyte affinity	Improved rate performance and surface-controlled capacitive behavior	Excess O groups may trigger side reactions and unstable SEI formation

Table 2. *Cont.*

Doping	Core Principle	Key Characteristics	Main Effect	Trade-Offs/Limitations
N/S	Tune the electronic structure and enlarge interlayer spacing	N enhances electrical conductivity, while S introduces local polarization	Extended cycling stability with a defect-rich framework	Increased ion storage sites and mitigated volume strain
O/F	Adjust K^+ E_{ads} and expand interlayer spacing	F adjusts electronic hybridization, while O improves surface wettability	Rapid reaction kinetics and a stable, uniform SEI layer	Promotes ion insertion while reducing irreversible capacity loss
B	Enhance π-electron activity and generate electron-deficient sites	Tune the electronic structure and expand interlayer distance	Accelerated charge transport with minimized volume expansion	-
O	Enhance surface wettability and introduce additional K^+ storage sites	Introduce oxygen-functional groups to improve interfacial reactivity	Enhanced ion transfer and formation of a stable SEI layer	-
N	Enhance electronic conductivity and introduce additional active sites	Create structural defects and fine-tune K^+ E_{ads}	Excellent rate performance and durable cycling stability	-
P	Reinforce the C framework while generating additional storage sites	Generate P-C and P-O bonds to expand interlayer distance	Enhanced capacity while maintaining structural integrity	-
S	Generate polarized sites and increase interlayer spacing	Strong electronegativity contrast helps mitigate volume changes	Facilitated K^+ diffusion and improved redox behavior	-

While heteroatom doping is widely recognized for enhancing the electrochemical performance of HC anodes, it often leads to a decrease in ICE. This is primarily attributed to the increased surface area and defect density introduced by doping, which promote irreversible side reactions, including electrolyte decomposition and the formation of SEI layers. Consequently, a portion of K-ions becomes irreversibly consumed during the initial cycles. In addition, excessive doping may further aggravate these effects, leading to reduced cycling CE. Therefore, achieving an optimal balance between enhanced capacity and high Coulombic efficiency remains a key challenge in the design of heteroatom-doped HC materials. Based on the above discussion, several key mechanistic design principles for heteroatom-doped HC can be identified: (i) heteroatoms with higher electronegativity differences induce charge redistribution and enhance K^+ adsorption; (ii) larger atomic radius dopants contribute to interlayer expansion and facilitate ion diffusion; (iii) controlled defect engineering increases active sites but must be balanced to maintain structural integrity; and (iv) synergistic multi-heteroatom doping enables simultaneous optimization of conductivity, adsorption energetics, and structural stability. These insights provide a rational framework for the design of next-generation HC anodes for PIBs.

Moreover, heteroatom doping plays a crucial role in determining the dominant K^+ storage mechanisms in HC. Electron-rich dopants such as N introduce defect sites and enhance charge density, thereby promoting surface adsorption and capacitive storage, which mainly contribute to the sloping region of the voltage profile. In contrast, larger heteroatoms such as P and S expand the interlayer spacing and facilitate K^+ intercalation, contributing to the low-voltage plateau capacity. Microporous structures are closely associated with pore filling mechanisms, whereas mesopores primarily serve as ion transport channels. Additionally, dopant-induced surface polarity significantly influences SEI formation, affecting interfacial stability and ICE. Therefore, the interplay

between dopant chemistry, pore structure, and electronic properties governs the overall K^+ storage behavior in HC materials.

5. Conclusions and Future Perspectives

Significant advancements in anode design, notably through heteroatom doping of hard carbons, have enhanced the overall behavior of PIBs. Transitions from single- to multi-element incorporation strategies have yielded enhancements in conductivity, K^+ diffusion kinetics, electrochemical rate capability, and cycle durability, underscoring the potential of PIBs as practical alternatives to LIBs in grid storage, EVs, and portable applications.

Single-heteroatom incorporation has been shown to address intrinsic limitations of pristine hard carbons. Elements including N, B, S, O, and P not only enhance conductivity but also introduce extra active sites for K^+ intercalation. By generating localized electron-rich or electron-deficient domains, these dopants improve charge transport. Additionally, tuning the pore structure and surface chemistry enhances the accessibility of K^+ storage positions, promoting faster diffusion and higher rate capability. Nonetheless, single-element incorporation generally only optimizes specific performance aspects, constraining its overall effectiveness in high-performance PIBs.

The co-introduction of multiple heteroatoms into HC frameworks provides an integrated strategy to exploit synergistic interactions among dopants. Dual- or tri-element combinations, for instance N/P or N/S, can concurrently boost conductivity, K^+ transport, and structural integrity due to complementary functions of each dopant. Nonetheless, realizing the full potential of multi-heteroatom doping requires careful control of dopant homogeneity, as uneven distribution may lead to localized performance loss, underutilization of active channels, and accelerated deterioration. Advanced synthesis approaches are therefore necessary to ensure uniform dopant dispersion and maximize synergistic effects.

Promising approaches to improve dopant precision include molecular-scale precursor engineering, such as the use of MOFs or heteroatom-rich polymers, as well as advanced processing approaches such as ALD and spray pyrolysis. Compared with single-element doping, the incorporation of multiple dopants into HC introduces substantially greater complexity, requiring precise control over precursor selection, dopant ratios, and reaction parameters. This increased complexity adversely affects synthesis reproducibility and raises production costs, thereby limiting large-scale implementation. Consequently, the development of simplified, cost-effective, and efficient multi-element doping strategies is essential for commercial viability. Despite the precise control offered by laboratory-scale doping approaches, their low throughput and elevated costs present significant obstacles to industrial implementation. Bridging this gap requires the development of scalable, high-yield doping strategies that maintain electrochemical performance. Moreover, practical application of doped HC anodes in PIBs is challenged by high mass loadings, which can impair ion and electron transfer and exacerbate volume expansion. Addressing these issues demands the construction of mechanically robust, conductive electrode architectures and systematic evaluation under commercially pertinent conditions.

Despite remaining limitations, multi-element-doped HC exhibits considerable promise for PIB applications. Continued advances in materials design and mechanistic understanding are expected to further refine its electrochemical behavior, extending the performance limits of PIBs and enhancing their competitiveness in large-scale energy storage. Several prospective research directions are summarized in Figure 17.

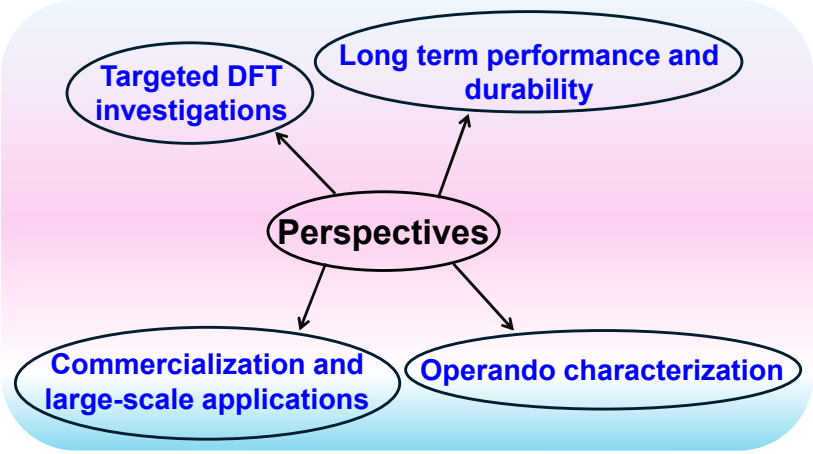

Figure 17. Schematic overview highlighting future research pathways and development prospects for doped HC anodes.

(1) DFT-guided materials optimization: The rational design of multi-heteroatom-doped C anodes demands a synergistic approach combining theoretical modeling with high-throughput computational and experimental techniques. Automated synthesis platforms and fast electrochemical characterization facilitate efficient exploration of dopant types, concentrations, and processing parameters. Machine learning approaches, including supervised learning and graph neural networks, allow correlations between key descriptors, for instance, dopant electronegativity, ionic radius, interlayer distance, defect density, charge redistribution, and K^+ E_{ads}, and electrochemical performance. These predictive frameworks should be grounded in first-principles calculations, with DFT studies quantifying synergistic K^+ adsorption, defect and dopant evolution, interfacial SEI stability, and the interplay between interlayer expansion and volumetric capacity.

(2) Operando characterization techniques: Addressing the debate between intercalation and pore-filling in multi-heteroatom incorporated HC necessitates advanced operando characterization. High-resolution operando XRD can quantify interlayer spacing variations during cycling, enabling the discrimination of lattice expansion caused by ion intercalation from pore-filling processes that do not modify layer spacings. Operando TEM integrated with EDS permits direct visualization of K^+ spatial distribution, revealing preferential occupancy of graphitic layers versus microporous regions. Concurrently, operando Raman analysis tracks changes in D- and G-band features, distinguishing intercalation-induced structural rearrangements from defect-related adsorption. Operando NMR further resolves the local chemical environment of K^+, differentiating adsorbed species from intercalated ones. Integrating these techniques provides a robust methodology to identify dominant K^+ storage mechanisms in multi-doped HC materials.

(3) Commercial deployment and scale-up: The development of multi-heteroatom doped HC has substantially enhanced its appeal for large-scale energy storage applications, such as grid systems, electric transportation, and renewable energy integration. PIBs incorporating these high-performance doped HC anodes present a viable and cost-efficient alternative to LIBs due to the abundance of K and favorable environmental considerations. Continued refinement of doping strategies is anticipated to further elevate PIB performance, positioning them as critical components in the advancement of sustainable energy infrastructures.

(4) Durability and long-term stability: Achieving robust long-term cycling behavior remains a critical prerequisite for the practical adoption of numerous heteroatom-

doped HC anodes in PIBs. Systematic evaluation of structural integrity under extended cycling is necessary, as repeated volume fluctuations during potassiation and depotassiation can trigger mechanical degradation. Future research should prioritize enhancing the mechanical resilience of doped HC, mitigating particle fracture and contact loss, thereby extending cycle life and ensuring reliable long-term electrochemical properties.

From a practical perspective, future research on HC anodes for PIBs should move beyond material-level optimization toward electrode-level and full-cell evaluation. Key metrics such as high mass loading (typically >2–3 mg cm^{-2}), high electrode density, and areal capacity (>2 mAh cm^{-2}) are essential to assess realistic performance but are often underreported. In addition, ICE remains a critical bottleneck for practical application due to irreversible K consumption during SEI formation. Furthermore, full-cell studies should be emphasized to validate the feasibility of HC anodes under practical conditions. This includes appropriate cathode matching, optimization of the N/P ratio, electrolyte engineering for stable SEI formation, and evaluation of long-term cycling stability under limited electrolyte conditions. Addressing these factors will be crucial for translating the promising properties of heteroatom-doped HC materials into commercially viable PIBs.

In summary, the evolution from single to numerous heteroatom doping strategies in HC has led to pronounced enhancements in PIB behavior. This shift from isolated dopant effects to synergistic structural engineering enables the simultaneous optimization of electronic conductivity, ion transport behavior, and mechanical robustness, thereby mitigating the inherent trade-offs of single-dopant systems. These advances significantly strengthen the competitiveness of PIBs relative to LIBs, particularly for large-scale applications where economic and sustainability considerations are critical. Continued refinement of heteroatom co-doped HC architectures is expected to position them as a key materials platform for next-generation energy storage technologies.

Author Contributions: Conceptualization, N.K.; formal analysis, N.K.; investigation, N.K.; resources, H.H., S.M. and A.L.F.d.B.; data curation, N.K., H.H., S.M. and A.L.F.d.B.; writing—original draft preparation, N.K.; writing—review and editing, N.K., H.H., S.M. and A.L.F.d.B.; visualization, N.K.; supervision, N.K., H.H., S.M. and A.L.F.d.B.; project administration, H.H., S.M. and A.L.F.d.B.; funding acquisition, H.H., S.M. and A.L.F.d.B. All authors have read and agreed to the published version of the manuscript.

Funding: This research was supported by the Nano and Material Technology Development Program through the National Research Foundation (NRF) of Korea, funded by the Ministry of Science and ICT (RS-2024-00449682). The authors acknowledge the financial support from the National Research Foundation of Korea (NRF) funded by the Ministry of Science and ICT (RS-2024-00433118). This research was supported by the National Research Foundation (NRF) of Korea, funded by the Government of Korea (MSIT) (RS-2023-00236572).

Data Availability Statement: Data sharing is not applicable to this article, as no datasets were generated or analyzed during the current study.

Conflicts of Interest: None of the authors has conflicts of interest to disclose.

References

1. Kitchamsetti, N.; Mhin, S. Synergistic Design of MXene Architectures for Mechanically Robust and High-Performance Flexible Batteries and Supercapacitors. *EcoEnergy* **2025**, *3*, e70018. [CrossRef]
2. Kitchamsetti, N.; Kim, K.; Han, H.; Mhin, S. Unveiling K-storage mechanisms in Te-based electrodes for potassium-ion batteries. *J. Energy Storage* **2026**, *144*, 119817. [CrossRef]

3. Li, M.; Wang, C.; Wang, C.; Lyu, Y.; Wang, J.; Xia, S.; Mao, J.; Guo, Z. 10 Years Development of Potassium-Ion Batteries. *Adv. Mater.* **2025**, *37*, 2416717. [CrossRef] [PubMed]
4. Cheng, L.; Quan, J.H.; Li, H.Y. Recent advances in antimony-based anode materials for potassium-ion batteries: Material selection, structural design and storage mechanisms. *Chin. Chem. Lett.* **2025**, *36*, 110685. [CrossRef]
5. Kitchamsetti, N.; de Barros, A.L.F.; Mhin, S. Transition Metal Nitrides: Multifunctional Catalysts and Energy Materials with Tailorable Architectures. *Small Sci.* **2025**, *5*, 2500331. [CrossRef] [PubMed]
6. Guo, Q.; Han, S.; Lu, Y.; Xiao, R.; Li, J.; Hao, Q.; Rong, X.; Weng, S.; Niu, Y.; Ding, F.; et al. Cation-self-shielding strategy promises high-voltage all-Prussian-blue-based aqueous K-ion batteries. *Nat. Commun.* **2025**, *16*, 4707. [CrossRef]
7. Xia, M.T.; Zhou, J.; Lu, B. Comprehensive Insights into Aqueous Potassium-Ion Batteries. *Adv. Energy Mater.* **2025**, *15*, 2404032. [CrossRef]
8. Kitchamsetti, N.; de Barros, A.L.F.; Han, H.; Mhin, S. Shaping the Future of Energy Storage with Single-Atom Materials. *J. Alloys Compd.* **2025**, *1044*, 184389. [CrossRef]
9. Wen, J.; Fu, H.; Gao, C.; Zhou, J.; Rao, A.M.; Wen, S.; Lu, B. Synergy Between Weak Solvent and Solid Electrolyte Interphase Enables High-Rate and Temperature-Resilient Potassium Ion Batteries. *Angew. Chem. Int. Ed.* **2025**, *64*, e202501155. [CrossRef]
10. Zhao, D.; Ding, M.; Tao, M.; Shan, P.; Lin, H.; Chen, Y.; Chen, J.; Zhou, Y.; Yang, Y. Advanced Interfacial Engineering of Graphite Anodes for Next-Generation Lithium-Ion Batteries. *Small* **2026**, *22*, e12150. [CrossRef] [PubMed]
11. Li, Q.; He, W.; Li, M.; Luo, J.; Yan, W.; Wu, D.; Zhang, Z.; Guo, C.; Yi, C.; Chen, L.; et al. All Solid State Battery with Soft Carbon-TiSi2 Multilayer Structure for Optimized LiSi Anodes. *Adv. Mater.* **2026**, *38*, e12753. [CrossRef] [PubMed]
12. Kitchamsetti, N.; Mhin, S.; Han, H. Intrinsic vacancy chemistry in Prussian white cathodes: Origins, multiscale characterization, and electrochemical consequences. *J. Energy Storage* **2026**, *160*, 121958. [CrossRef]
13. Manna, S.; Billa, R.; Puravankara, S. One anode, three ions: Mechanistic distinctions of Li plus, Na plus, and K plus storage in commercial hard carbon for alkali-ion batteries. *J. Power Sources* **2026**, *667*, 239235. [CrossRef]
14. Zhang, Z.; Qi, W.; Zhang, S.; Zhu, J.; Wang, L.; Bai, Y.; Chen, J.; Chen, Y.; Hou, G.; Niu, X.; et al. Solvation Geometry Engineering for Stable High-Voltage Potassium-Ion Batteries. *Energy Environ. Sci.* **2026**, *19*, 1374–1384. [CrossRef]
15. Kitchamsetti, N.; Mhin, S. Advances and Prospects of Lignin-Derived Hard Carbons for Next-Generation Sodium-Ion Batteries. *Polymers* **2025**, *17*, 2801. [CrossRef] [PubMed]
16. Liu, J.; Huang, L.; Wang, H.; Sha, L.; Liu, M.; Sun, Z.; Gu, J.; Liu, H.; Zhao, J.; Zhang, Q.; et al. The Origin, Characterization, and Precise Design and Regulation of Diverse Hard Carbon Structures for Targeted Applications in Lithium-/Sodium-/Potassium-Ion Batteries. *Electrochem. Energy Rev.* **2024**, *7*, 34. [CrossRef]
17. Kitchamsetti, N.; Kim, K.; Han, H.; Mhin, S. Biomass-Derived Hard Carbon Anodes for Sodium-Ion Batteries: Recent Advances in Synthesis Strategies. *Nanomaterials* **2025**, *15*, 1554. [CrossRef]
18. Kundu, M.; Konar, R.; Maiti, S. Potassium-Ion Battery Anodes: Mechanistic Frameworks, Electrolyte/Binder Integration, and Roadmap Toward Commercialization. *Adv. Energy Mater.* **2026**, *16*, e05727. [CrossRef]
19. Kitchamsetti, N.; Mannem, C.K.; Chakra, C.S.; de Barros, A.L.F. A review of the exploration of nanostructured electrode materials, electrolytes, and performance in metal-ion (Li, Na, K, and Zn) hybrid capacitors. *J. Energy Storage* **2025**, *106*, 114836. [CrossRef]
20. Kitchamsetti, N.; Payyavula, S.; Cho, J.S. A review on hollow nanostructures, its derived composites: Preparation, structural control, alterations, and their utilization as an electrode for supercapacitors, rechargeable batteries and electrocatalysis. *J. Energy Storage* **2024**, *98*, 113143. [CrossRef]
21. Zhang, K.Y.; Liu, H.H.; Gu, Z.Y.; Yang, J.L.; Wang, X.Y.; Zhe, R.J.; Wang, Y.; Wu, X.L. Modeling Electrochemical Na/K-Storage Behaviors of Carbonaceous Materials. *Chem. Rev.* **2025**, *125*, 11145–11215. [CrossRef]
22. Kitchamsetti, N.; Mhin, S. Engineering cathodes and separators with zeolitic imidazolate frameworks-derived materials for advanced lithium-sulfur batteries. *J. Alloys Compd.* **2025**, *1046*, 184742. [CrossRef]
23. Kitchamsetti, N.; Mannem, C.K. A review on preparation of metal tellurides and their utilization as an electrode for supercapacitors, rechargeable batteries and electrocatalysis. *J. Alloys Compd.* **2025**, *1027*, 180664. [CrossRef]
24. Lanero, F.; Giulian, A.D.; Scettri, A.; Magnano, E.; Píš, I.; Azcona, I.N.; Casella, G.; Carlotto, S.; Moretti, E.; Carturan, S.M.; et al. Valorizing Coffee Waste into N-, P-, O-Heteroatom-Doped Carbons for Metal-Free Electrocatalysis. *Chem. Mater.* **2026**, *38*, 336–350. [CrossRef]
25. Zhang, M.; Hu, M.; Liu, X.; Zhang, Y.; Yuan, X.; Zhang, Z.; Xiong, K.; Zhang, W.; Xu, Q.; Ren, Z.; et al. Tailoring heteroatom-doped porous carbon materials for efficient adsorption of volatile organic compounds: Fabrication strategies, doping effects, and adsorption mechanisms. *Coord. Chem. Rev.* **2026**, *547*, 217155. [CrossRef]
26. Kitchamsetti, N.; Cho, J.S. A roadmap of recent advances in MXene@ MOF hybrids, its derived composites: Synthesis, properties, and their utilization as an electrode for supercapacitors, rechargeable batteries and electrocatalysis. *J. Energy Storage* **2024**, *80*, 110293. [CrossRef]
27. Yang, F.; Liu, Z.; Wang, D.; Hui, K.N.; Zhang, Y.; Peng, Z. Preparation and Properties of P-Bi_2Te_3/MXene Superstructure-based Anode for Potassium-Ion Battery. *Acta Phys. Chim. Sin.* **2024**, *40*, 2303006. [CrossRef]

28. Gu, Y.; Pei, Y.R.; Zhao, M.; Wang, G.Y.; Yang, C.C.; Jiang, Q. N-Doped Carbon Nanonecklaces as a Potassium-Ion Battery Anode. *ACS Appl. Nano Mater.* **2023**, *6*, 19896–19904. [CrossRef]
29. Lee, J.S.; Kitchamsetti, N.; Cho, J.S. Hierarchical porous nanofibers comprising N-doped graphitic C and ZIF-8 derived hollow N-doped C nanocages for long-life K-ion battery anodes. *Chem. Eng. J.* **2024**, *487*, 150465. [CrossRef]
30. Liu, Z.; Gong, Z.; He, K.; Qiu, P.; Wang, X.C.; Zhao, L.K.; Gu, Q.F.; Gao, X.W.; Luo, W.B. Developments and prospects of carbon anode materials in potassium-ion batteries. *Sci. China Mater.* **2025**, *68*, 709–723. [CrossRef]
31. Kitchamsetti, N.; de Barros, A.L.F.; Han, H.; Mhin, S. Unveiling MBenes: A New Class of 2D Materials Shaping the Future of Energy. *Adv. Sustain. Syst.* **2025**, *9*, e00581. [CrossRef]
32. Liao, J.; Sheng, X.; Yuan, Z.; Wang, Y.; Tu, F.; Qi, H.; Zhou, C.; Hu, Q.; Zhou, X. K^+ Vacancies and Fluorine Substitution Synergistically Regulate $KTiOPO_4$ Anode for All-Climate and Long-Life Potassium-Ion Batteries. *Angew. Chem. Int. Ed.* **2025**, *64*, e202516467. [CrossRef] [PubMed]
33. Lee, J.S.; Baek, K.W.; Kitchamsetti, N.; Kim, H.W.; Cho, J.S. Prussian blue analogue-derived porous nanocages with hollow (Co, Fe)O nanoparticles as anodes for lithium ion batteries. *J. Mater. Sci. Technol.* **2025**, *223*, 76–90. [CrossRef]
34. Kitchamsetti, N.; Narsimulu, D.; Payyavula, S.; Chakra, C.S.; de Barros, A.L.F. V-MOF derived porous nanorods comprising polydopamine-derived C coated VN quantum dots composited with graphitic C as electrodes for long-lasting and high-rate lithium-ion batteries and hybrid supercapacitors. *J. Energy Storage* **2025**, *109*, 115144. [CrossRef]
35. Li, W.; Bi, Z.; Zhang, W.; Wang, J.; Rajagopalan, R.; Wang, Q.; Zhang, D.; Li, Z.; Wang, H.; Wang, B. Advanced cathodes for potassium-ion batteries with layered transition metal oxides: A review. *J. Mater. Chem. A* **2021**, *9*, 8221–8247. [CrossRef]
36. Tang, H.; Lu, Z.; Yuan, Z.; Duan, L.; Zhang, Y.; Zhou, X.; Lin, Y.; Zhou, H. Optimizing Electronic Structure to Achieve High-Capacity and Long-Life Layered Oxide Cathode for Potassium-Ion Batteries. *Angew. Chem. Int. Ed.* **2025**, *64*, e202511899. [CrossRef]
37. Zhang, B.; Choi, Y.J.; Zhu, Z.; Zhao, S.Q.; Guo, S. Manganese-Based Layered Oxide Cathodes for Potassium-Ion Batteries: Progress and Outlook. *Adv. Energy Mater.* **2025**, *16*, 2501657. [CrossRef]
38. Liu, T.T.; Shi, P.C.; Gao, Y.; Chen, J.; Cheng, X.; Tao, X.; Sun, Z.; Huang, F.; Jiang, Y. Regulating interfacial chemistry toward highly reversible potassium-metal anodes in carbonate electrolytes. *J. Energy Chem.* **2025**, *111*, 211–219. [CrossRef]
39. Li, Y.; Zhang, F.; Cui, Y.; Guo, Y.; Yang, A.; Wang, X. Steric-confined coordination engineering of weakly solvating electrolyte enables stable interfacial chemistry for potassium metal/ion batteries. *Chem. Eng. J.* **2025**, *524*, 169269. [CrossRef]
40. He, Y.; Liu, D.; Li, Q.; Zhu, Z.; Wu, R. Advances in oxygen-containing functional groups-modified hard carbon anodes for sodium-ion batteries. *Mater. Sci. Eng. R Rep.* **2026**, *168*, 101143. [CrossRef]
41. Huang, W.; Wu, C.; Zhong, L.; Chen, Q.; Zhang, H.; Tan, X.; Chou, S.; Wu, X. Unlocking Kinetic Limitations in Hard-Carbon Anodes to Enable Practical Fast-Charging Sodium-Ion Batteries. *Adv. Energy Mater.* **2026**, *16*, e05568. [CrossRef]
42. Gao, Y.; Ma, X.; Yan, Y.; Zhang, S.; Liang, J.; Li, B.; Kang, F.; Zhai, D. Unleashing the Underestimated Rate Capability of Graphite Anode for Potassium-Ion Batteries by $Sn(OTf)_2$ Electrolyte Additive. *Adv. Energy Mater.* **2025**, *15*, 2404913. [CrossRef]
43. Gao, L.; Zeng, J.; Ge, X.; Gao, T.; Wang, Y.; Sun, Z.; Deng, D.; Qiu, Y.; Wang, L.; Jiang, X.; et al. Biomass-Derived Carbon with Heavy Doping for Anode of Potassium Ion Batteries. *Adv. Mater.* **2026**, *38*, e20046. [CrossRef]
44. Li, F.; Mo, F.; Zhong, C.; Chen, Y.; Liu, Z.; Duan, Y.; Ma, X.; Fan, Y.; Dong, X.; Chen, Z.; et al. A roadmap toward high-performance hard carbon for sodium-ion batteries: From fundamental studies on synthesis and mechanism to practical application. *Energy Storage Mater.* **2025**, *83*, 104668. [CrossRef]
45. Yu, H.; Liu, X.; Zhang, Z.; Wu, Y.; Chen, D.; Huang, J.; Wu, Y.; Chen, Y.; He, J. Engineering Pseudo-Graphite-Dominated Hard Carbon as Anode for Sodium-Ion Batteries. *ACS Energy Lett.* **2025**, *10*, 4342–4352. [CrossRef]
46. Kitchamsetti, N.; Cho, J.S.; Chakra, C.S. Prussian blue analogue derived porous hollow nanocages comprising polydopamine-derived N-doped C coated $CoSe_2/FeSe_2$ nanoparticles composited with N-doped graphitic C as an anode for high-rate Na-ion batteries. *Chem. Eng. J.* **2024**, *495*, 153353. [CrossRef]
47. Zhou, W.; Mo, Y.; Zheng, B.; Wu, Y.; Li, X.; Liu, Z.; Ke, Y.; Chen, S.; Gao, P.; Duan, Y.; et al. Scalable Steam-Assisted Pyrolysis for Hard Carbon Anodes Toward High-Performance Alkali-Ion Storage. *Adv. Funct. Mater.* **2026**, e32130. [CrossRef]
48. Yang, Q.; Zhou, X.; Huang, T.; Chen, Z.; Zhang, Y.; Shi, S.; Zhang, W.; Li, L.; Wang, J.; Dou, S.; et al. Latent Solvent-Induced Inorganic-Rich Interfacial Chemistry to Achieve Stable Potassium-Ion Batteries in Low-Concentration Electrolyte. *Angew. Chem.-Int. Ed.* **2025**, *64*, e202422259. [CrossRef]
49. Zhou, W.; Wang, D.; Mo, Y.; Tang, R.; Gao, P.; Han, M.M.; Chen, S.; Wakabayashi, K.; Yoshii, T.; Nishihara, H.; et al. Tuning surface reactivity towards high-performance hard carbon in Li/Na/K-ion batteries. *J. Energy Chem.* **2025**, *103*, 27–36. [CrossRef]
50. Kitchamsetti, N.; de Barros, A.L.F.; Mhin, S. Prussian Blue Analogs as Cathode Materials for Sodium-Ion Batteries. *Batter. Supercaps* **2025**, *8*, e202500482. [CrossRef]
51. Yang, L.; Jiang, W.; Wang, X.; Ren, W.; Wang, H. Synergistic structural engineering and fluorine doping strategy in hard carbon for fast and stable potassium-ion storage. *J. Energy Storage* **2026**, *146*, 120059. [CrossRef]

52. Zhao, R.; Wang, Y.; Zhang, Z.Y.; Fan, X.; Chen, H.G.; Jing, R.; Ma, L.; Peng, H. Dual modulation of pore architecture and surface chemistry in P, N co-doped carbons for high-performance potassium ion hybrid capacitors. *J. Energy Storage* **2026**, *152*, 120793. [CrossRef]
53. Yao, Y.; Qi, E.; Sun, M.; Wei, Z.; Jiang, H.; Du, F. Unlocking the potential of potassium-ion batteries: Anode material mechanisms, challenges, and future directions. *Nanoscale* **2025**, *17*, 19021–19054. [CrossRef]
54. Li, Y.; Wu, S.; Chen, L.; Fan, H.; Zhang, Y.; Zeng, L. Multiple yolks-shell cobalt phosphosulfide nanocrystals encapsulating into rich heteroatoms co-doped carbon frameworks for advanced sodium/potassium ion batteries. *Chin. Chem. Lett.* **2025**, *36*, 110371. [CrossRef]
55. Wu, S.; Li, Y.; Chen, L.; Zhang, Y.; Zeng, L.; Fan, H. Hexapod cobalt phosphosulfide nanorods encapsulating into multiple hetero-atom doped carbon frameworks for advanced sodium/potassium ion battery anodes. *Chin. Chem. Lett.* **2025**, *36*, 109796. [CrossRef]
56. Pan, J.; Sun, Z.; Wu, X.; Liu, T.; Xing, Y.; Chen, J.; Xue, Z.; Tang, D.; Dong, X.; Zhang, H.; et al. Mechanically Robust Bismuth-Embedded Carbon Microspheres for Ultrafast Charging and Ultrastable Sodium-Ion Batteries. *J. Am. Chem. Soc.* **2025**, *147*, 3047–3061. [CrossRef] [PubMed]
57. Yang, H.; Liu, F.; Zou, X.; Jiang, Z.; Zhou, X.; Wu, X.; Qiao, S.; Zhang, W.; Zheng, W. B-doping tunes surface chemistry of graphite cathode interfaced at electrolyte for optimal anion storage and robust dual-ion batteries. *Acta Mater.* **2025**, *285*, 120692. [CrossRef]
58. Zheng, P.; Zhou, W.; Mo, Y.; Zheng, B.; Han, M.; Zhong, Q.; Yang, W.; Gao, P.; Yang, L.; Liu, J. Multi boron-doping effects in hard carbon toward enhanced sodium ion storage. *J. Energy Chem.* **2025**, *100*, 730–738. [CrossRef]
59. Jiang, Y.; Xiao, N.; Song, X.; Xiao, J.; Yu, K.; Dai, X.; Lv, Z.; Qiu, J. Coal Tar Pitch Derived sp^2 Configuration-Dominated Vacancy-Rich Carbon with Expand Interlayer Spacing for Low-Voltage, Durable, and Fast Potassium Storage. *Adv. Funct. Mater.* **2024**, *34*, 2316207. [CrossRef]
60. Berenjaghi, H.M.; Mansouri, S.; Beheshtian, J. A DFT study on the potential application of pristine, B and N doped carbon nanocones in potassium-ion batteries. *J. Mol. Model.* **2021**, *27*, 168. [CrossRef]
61. Lu, J.F.; Li, K.C.; Lv, X.Y.; Kuai, H.X.; Su, J.; Wen, Y.X. Boron-Doped Pine-Cone Carbon with 3D Interconnected Porosity for Use as an Anode for Potassium-Ion Batteries with Long Life Cycle. *Front. Chem.* **2022**, *10*, 953782. [CrossRef]
62. Feng, B.J.; Liu, J.J.; Wu, X.H.; Gu, Z.Q.; Liu, L.Z.; Yang, L.B.; Dai, C.; Han, K.; Zhao, M.J.; Jiang, W.J.; et al. An agro-bionic approach to co-chelating ultrafine high-entropy metal phosphosulfide nanoparticles for superior Li/K-ion storage. *Chem. Eng. J.* **2026**, *529*, 173061. [CrossRef]
63. Jiang, R.; Huang, J.; Ma, R.; Li, Q.; Dai, L.; Li, R.; Chen, X.; Ren, Y.; Liu, Z.; Chen, X.; et al. Construction of Sb_2S_3@NC Core-Shell Nanorod with Hollow Feature as Anode via Microstructure Regulation Strategy for High-Performance Na^+/K^+ Storage. *J. Mater. Chem. A* **2026**, *14*, 10265–10278. [CrossRef]
64. Qin, M.; Chen, C.; Zhang, B.; Yan, J.; Qiu, J. Ultrahigh Pyridinic/Pyrrolic N Enabling N/S Co-Doped Holey Graphene with Accelerated Kinetics for Alkali-Ion Batteries. *Adv. Mater.* **2024**, *36*, 2407570. [CrossRef] [PubMed]
65. Yu, Q.; Shi, X.; Zhang, T.; Zhao, Y.; Jin, J.; Wang, R.; Gong, Y.; Wang, H. Hollow carbon fibers with balanced graphitization and defects for extremely fast-charging potassium storage. *Nano Res.* **2026**, *19*, 94908253. [CrossRef]
66. Zhou, Y.; Zhu, Y.; Liu, Y.; Xu, B. Topological Defect-Regulated Porous Carbon Nanoribbon for High-Performance Potassium-Ion Batteries. *Small* **2025**, *21*, 2408974. [CrossRef]
67. Wang, J.; Yuan, J.; Bai, L.; Xu, W.; Liu, X.; Liu, G.; Li, S.; Huang, Z.D. Doped Hard Carbon Nanotube Bundles for Superior Potassium Storage. *ACS Appl. Nano Mater.* **2025**, *8*, 13332–13339. [CrossRef]
68. Chen, C.; Wang, Z.; Zhang, B.; Miao, L.; Cai, J.; Peng, L.; Huang, Y.; Jiang, J.; Huang, Y.; Zhang, L.; et al. Nitrogen-rich hard carbon as a highly durable anode for high-power potassium-ion batteries. *Energy Storage Mater.* **2017**, *8*, 161–168. [CrossRef]
69. Zhao, L.; Yang, H.; He, F.; Yao, Y.; Xu, R.; Wang, L.; He, L.; Zhang, H.; Li, S.; Huang, F. Biomimetic N-doped sea-urchin-structured porous carbon for the anode material of high-energy-density potassium-ion batteries. *Electrochim. Acta* **2021**, *388*, 138565. [CrossRef]
70. Li, D.; Ren, X.; Ai, Q.; Sun, Q.; Zhu, L.; Liu, Y.; Liang, Z.; Peng, R.; Si, P.; Lou, J.; et al. Facile Fabrication of Nitrogen-Doped Porous Carbon as Superior Anode Material for Potassium-Ion Batteries. *Adv. Energy Mater.* **2018**, *8*, 1802386. [CrossRef]
71. Kitchamsetti, N.; de Barros, A.L.F.; Han, H.; Mhin, S. Recycling of Spent Cathode Carbon from Aluminum Electrolysis: Detoxification Approaches, Resource Utilization, and Environmental Perspectives. *ChemElectroChem* **2026**, *13*, e202500353. [CrossRef]
72. Kuai, J.; Xie, J.; Wang, J.D.; Chen, J.Y.; Wang, J.; Liu, F.; Xu, X.W.; Tu, J.; Cheng, J.P. Optimizing hard carbon materials for sodium-ion batteries: Insights from particle size and soft carbon-coating strategy. *J. Power Sources* **2025**, *627*, 235792. [CrossRef]
73. Zheng, J.; Wu, Y.; Tong, Y.; Liu, X.; Sun, Y.; Li, H.; Niu, L. High Capacity and Fast Kinetics of Potassium-Ion Batteries Boosted by Nitrogen-Doped Mesoporous Carbon Spheres. *Nano Micro Lett.* **2021**, *13*, 174. [CrossRef]
74. Jung, S.H.; Min, J.W.; Choi, H.; Mapari, M.; Chougale, M.; Dubal, D.P.; Kim, T.Y. Role of Mesoporosity in Hard Carbon Anodes for High-Energy and Stable Potassium-Ion Storage. *Small* **2025**, *21*, 2410232. [CrossRef] [PubMed]

75. Zhang, S.; Xu, Z.; Duan, H.; Xu, A.; Xia, Q.; Yan, Y.; Wu, S. N-doped carbon nanofibers with internal cross-linked multiple pores for both ultra-long cycling life and high capacity in highly durable K-ion battery anodes. *Electrochim. Acta* **2020**, *337*, 135767. [CrossRef]
76. Qiao, X.; Jin, G.; Liu, R.; Hou, J.; Shi, X.; Wang, L.; Tian, Q.; Lu, H.; Shen, Z.; Lan, Y.; et al. A Function-Oriented Binder with Exceptional Interface Ion Transport and Impurity Tolerance for Hard Carbon Anode. *Small* **2025**, *21*, 2500532. [CrossRef] [PubMed]
77. Yang, L.; Pang, H.; Ren, W.; Wang, X.; Wei, Y.; Lu, P.; Chen, J.; Tian, W.; Huang, M.; Wang, H. Joule Heating Driven Graphitization Regulation and Ni Single-Atom Modification in Hard Carbon for Low-Voltage and High-Rate Potassium-Ion Storage. *Adv. Funct. Mater.* **2026**, *36*, e16237. [CrossRef]
78. Hu, J.; Xie, Y.; Yin, M.; Zhang, Z. Nitrogen doping and graphitization tuning coupled hard carbon for superior potassium-ion storage. *J. Energy Chem.* **2020**, *49*, 327–334. [CrossRef]
79. Deng, W.; He, X.D.; Zhang, L.; Wang, J.; Chen, C. Highly Graphitic N-Doped Biomass-Derived Hard Carbon with a Low Operating Potential for Potassium-Ion Batteries. *Energy Technol.* **2021**, *9*, 2100644. [CrossRef]
80. Xiang, J.; Ma, L.; Sun, Y.; Dong, S.; Xu, Q.; He, X.; Zhou, Y.; Hai, C. Ball-Milling-Assisted N/O Codoping for Enhanced Sodium Storage Performance of Coconut-Shell-Derived Hard Carbon Anodes in Sodium-Ion Batteries. *Langmuir* **2024**, *40*, 23853–23863. [CrossRef] [PubMed]
81. Lu, X.; Zhou, J.; Li, X.; Peng, H.; Shi, C.; Liu, F.; Huang, L.; Sun, Z. In Situ Composite Strategy of O/F-Dual-Doped Soft-Hard Carbon Anode Promotes Ultrafast and Highly Durable Potassium Storage Performance. *ACS Appl. Mater. Interfaces* **2025**, *17*, 29708–29719. [CrossRef]
82. Shen, N.; Lai, Q.; Chen, N.; Pang, Y.; Chen, H.; Zhang, W.; Liu, Z. Hard Carbon Anode Synthesized by an In Situ Porous Strategy for Advanced Potassium-Ion Batteries. *ACS Sustain. Chem. Eng.* **2023**, *11*, 14572–14581. [CrossRef]
83. Wang, J.; Xu, Z.; Eloi, J.C.; Titirici, M.M.; Eichhorn, S.J. Ice-Templated, Sustainable Carbon Aerogels with Hierarchically Tailored Channels for Sodium- and Potassium-Ion Batteries. *Adv. Funct. Mater.* **2022**, *32*, 2110862. [CrossRef]
84. Qian, Y.; Jiang, S.; Li, Y.; Yi, Z.; Zhou, J.; Li, T.; Han, Y.; Wang, Y.; Tian, J.; Lin, N.; et al. In Situ Revealing the Electroactivity of P-O and P-C Bonds in Hard Carbon for High-Capacity and Long-Life Li/K-Ion Batteries. *Adv. Energy Mater.* **2019**, *9*, 1901676. [CrossRef]
85. Alvin, S.; Chandra, C.; Kim, J. Extended plateau capacity of phosphorus-doped hard carbon used as an anode in Na- and K-ion batteries. *Chem. Eng. J.* **2020**, *391*, 123576. [CrossRef]
86. Tang, Z.; Liu, Y.; Song, S.; Liu, Z. Sulfur-doped hollow carbon spheres as high-performance anode materials for potassium-ion batteries. *J. Alloys Compd.* **2025**, *1031*, 180976. [CrossRef]
87. Cao, B.; Guo, Z.; Liu, H.; Ma, Y.; Zhao, W.; Yang, Y.; Li, A.; Song, H.; Yang, Y.; Li, Z.; et al. High content of single-atomic sulfur in nano carbon spheres boosting potassium storage performance. *Chem. Eng. J.* **2025**, *511*, 161950. [CrossRef]
88. Kim, H.J.; Lim, J.B.; Na, J.H.; Kim, J.K.; Yoo, Y.; Kang, Y.C.; Park, S.K. Sulfur-doped pomegranate-like carbon microclusters designed via facile spray-drying process: A novel anode material for potassium-ion batteries. *Appl. Surf. Sci.* **2024**, *675*, 160973. [CrossRef]
89. Sun, T.; Huang, F.; Liu, J.; Yu, H.; Feng, X.; Feng, X.; Yang, Y.; Shu, H.; Zhang, F. Strengthened d-p Orbital-Hybridization of Single Atoms with Sulfur Species Induced Bidirectional Catalysis for Lithium-Sulfur Batteries. *Adv. Funct. Mater.* **2023**, *33*, 2306049. [CrossRef]
90. Qiu, C.; Kumar, A.; Tabish, M.; Mai, X.; Guo, L.; Zhao, Y.; Zhu, Y.; Li, A.; Yasin, G.; Chen, X.; et al. Sulfur-bonded hard carbon with enhanced interfacial and bulk kinetics for potassium-ion hybrid capacitors. *Chem. Eng. J.* **2025**, *517*, 164446. [CrossRef]
91. Sun, Q.; Mu, J.; Ma, F.; Li, Y.; Zhou, P.; Zhou, T.; Wu, X.; Zhou, J. Sulfur-doped hollow porous carbon spheres as high-performance anode materials for potassium ion batteries. *J. Energy Storage* **2023**, *72*, 108297. [CrossRef]
92. Huang, Y.; Hu, X.; Li, Y.; Zhong, X.; He, Z.; Geng, Z.; Gan, S.; Deng, W.; Zou, G.; Hou, H.; et al. Demystifying the Influence of Precursor Structure on S-Doped Hard Carbon Anode: Taking Glucose, Carbon Dots, and Carbon Fibers as Examples. *Adv. Funct. Mater.* **2024**, *34*, 2403648. [CrossRef]
93. Chen, X.Y.; Cheng, X.B.; Liu, Z.G. High sulfur-doped hard carbon anode from polystyrene with enhanced capacity and stability for potassium-ion storage. *J. Energy Chem.* **2022**, *68*, 688–698. [CrossRef]
94. Chi, C.; Liu, Z.; Lu, X.; Meng, Y.; Huangfu, C.; Yan, Y.; Qiu, Z.; Qi, B.; Wang, G.; Pang, H.; et al. Balance of sulfur doping content and conductivity of hard carbon anode for high-performance K-ion storage. *Energy Storage Mater.* **2023**, *54*, 668–679. [CrossRef]
95. Qiu, D.; Zhang, B.; Zhang, T.; Shen, T.; Zhao, Z.; Hou, Y. Sulfur-Doped Carbon for Potassium-Ion Battery Anode: Insight into the Doping and Potassium Storage Mechanism of Sulfur. *ACS Nano* **2022**, *16*, 21443–21451. [CrossRef]
96. Huang, R.; Zhang, X.; Qu, Z.; Zhang, X.; Lin, J.; Wu, F.; Chen, R.; Li, L. Defects and sulfur-doping design of porous carbon spheres for high-capacity potassium-ion storage. *J. Mater. Chem. A* **2022**, *10*, 682–689. [CrossRef]
97. Li, Y.; Zhu, A.; Peng, G.; He, J.; Li, H.; Jia, D.; Qiu, J.; He, X. Confined soft carbon in hard carbon with enhanced ion transport kinetics as anode for high-rate and stable potassium-ion batteries. *J. Energy Chem.* **2025**, *103*, 97–105. [CrossRef]

98. Quan, Z.; Wang, F.; Wang, Y.; Liu, Z.; Zhang, C.; Qi, F.; Zhang, M.; Ye, C.; Tan, J.; Liu, J. Robust Micro-Sized and Defect-Rich Carbon-Carbon Composites as Advanced Anodes for Potassium-Ion Batteries. *Small* **2024**, *20*, 2305841. [CrossRef] [PubMed]
99. Sun, B.; Zhang, Q.; Xu, W.; Zhao, R.; Zhang, C.; Guo, J.; Zhu, H.; Yuan, G.; Lv, W.; Li, X.; et al. Edge-enriched and S-doped carbon nanorods to accelerate electrochemical kinetics of sodium/potassium storage. *Carbon* **2023**, *201*, 776–784. [CrossRef]
100. Liu, C.; Feng, X.; Zhao, Y.; Fan, H.; Zheng, R.; Wang, Z.; Arandiyan, H.; Wang, Y.; Bhargava, S.K.; Liu, Y.; et al. Enhancing potassium ions adsorption on mesoporous carbon spheres with abundant internal surface via engineering sulfur doping sites towards superior rate capability. *J. Colloid Interface Sci.* **2023**, *652*, 1325–1337. [CrossRef] [PubMed]
101. Liu, W.; Zhang, H.; Ye, W.; Xiao, B.; Sun, Z.; Cheng, Y.; Wang, M.S. Regulating the Wettability of Hard Carbon through Open Mesochannels for Enhanced K^+ Storage. *Small* **2023**, *19*, 2300605. [CrossRef]
102. Chattopadhyay, S.; Pramanik, A.; Pieshkov, T.; Chandrasekhar, G.; Alhashim, S.; Vajtai, R.; Ajayan, P.M. B, N Co-Doped Hard Carbon Nano-Sponge Enhancing Half and Full Cell Performance in Na-Ion Batteries. *Small* **2025**, *21*, 2500120. [CrossRef]
103. Jiang, C.; Li, Y.; Wan, C.; Wu, Q.; Yang, S.; Chen, K.; You, Y.; Tian, Y.; Huang, J.; Xie, H. Dual regulation of structure and interface enabled high-rate and high-capacity hard carbon anode for sodium-ion batteries. *Chem. Eng. J.* **2025**, *506*, 160124. [CrossRef]
104. Kandula, S.; Youn, B.S.; Cho, J.; Lim, H.K.; Son, J.G. FeS_2@N-C nanorattles encapsulated in N/S dual-doped graphene/carbon nanotube network composites for high performance and high rate capability anodes of sodium-ion batteries. *Chem. Eng. J.* **2022**, *439*, 135678. [CrossRef]
105. Muzammil, A.; Haider, R.; Wei, W.; Wan, Y.; Ishaq, M.; Zahid, M.; Yaseen, W.; Yuan, X. Emerging transition metal and carbon nanomaterial hybrids as electrocatalysts for water splitting: A brief review. *Mater. Horiz.* **2023**, *10*, 2764–2799. [CrossRef] [PubMed]
106. Liu, L.; Zhang, X.; Zhang, D.; Zhang, K.; Hou, S.; Wang, S.; Zhang, Y.; Peng, H.; Liu, J.; Yan, C. Regulating the N/B ratio to construct B, N co-doped carbon nanotubes on carbon felt for high-performance vanadium redox flow batteries. *Chem. Eng. J.* **2023**, *473*, 145454. [CrossRef]
107. Huang, Z.; Fang, M.; Yang, T.; Zheng, R.; Shen, T.; Ji, H.; Dong, C.; Zhou, J.; Zhang, J.; Zhang, X. A universal method for N/B codoped carbon bubbles for enhanced potassium ion storage. *Electrochim. Acta* **2024**, *476*, 143714. [CrossRef]
108. Chen, Y.; Fu, N.; Shen, B.; Yan, Y.; Shao, W.; Wang, T.; Xie, H.; Yang, Z. Edge coordination of Ni single atoms on hard carbon promotes the potassium storage and reversibility. *Small* **2023**, *19*, 2207423. [CrossRef]
109. Kitchamsetti, N.; Cho, J.S. A roadmap of MOFs derived porous carbon, oxides, chalcogenides, and phosphides of metals: Synthesis, properties, parameter modulation and their utilization as an electrode for Li/Na/K-ion batteries. *J. Energy Storage* **2024**, *84*, 110947. [CrossRef]
110. Kitchamsetti, N. A review on recent advances in Prussian blue, its analogues, and their derived materials as electrodes for high performance supercapacitors. *J. Energy Storage* **2023**, *73*, 108958. [CrossRef]
111. Kitchamsetti, N.; Kim, D. High performance hybrid supercapacitor based on hierarchical MOF derived $CoFe_2O_4$ and $NiMn_2O_4$ composite for efficient energy storage. *J. Alloys Compd.* **2023**, *959*, 170483. [CrossRef]
112. Kitchamsetti, N.; Kim, D. A facile method for synthesizing MOF derived $ZnCo_2O_4$ particles on MXene nanosheets as a novel anode material for high performance hybrid supercapacitors. *Electrochim. Acta* **2023**, *441*, 141824. [CrossRef]
113. Piao, J.; Seo, S.; Lee, S.; Lee, I.; Nurul, F.A.; Mathew, V.; Kim, J. Tin-carbon composite anode with nitrogen-doped porous framework for potassium-ion batteries. *J. Energy Storage* **2026**, *152*, 120635. [CrossRef]
114. Jiang, H.; Fu, Q.; Sang, X.; Qiu, H.; Liu, S.; Liu, Q.; Zhang, Y.; Lin, J.; Zhao, X. Solid Electrolyte Interphase Stabilized Pomegranate SnP_2O_7@PC Anodes Realized Through Kirkendall Effect of MOF for Durable Potassium/Sodium-Ion Batteries. *Adv. Energy Mater.* **2026**, *16*, e05082. [CrossRef]
115. Xia, G.; Wang, C.; Jiang, P.; Lu, J.; Diao, J.; Chen, Q. Nitrogen/oxygen co-doped mesoporous carbon octahedrons for high-performance potassium-ion batteries. *J. Mater. Chem. A* **2019**, *7*, 12317–12324. [CrossRef]
116. Yang, J.; Ju, Z.; Jiang, Y.; Xing, Z.; Xi, B.; Feng, J.; Xiong, S. Enhanced Capacity and Rate Capability of Nitrogen/Oxygen Dual-Doped Hard Carbon in Capacitive Potassium-Ion Storage. *Adv. Mater.* **2018**, *30*, 1700104. [CrossRef]
117. Wang, J.; Huang, Z.; Zhang, W.; Li, Q.; Liang, Z.; Lu, J.; Lin, Z.; Wang, G.; Wu, J.; Huang, S. Balancing Graphitic Nanodomains and Heteroatom Doping in Hard Carbons Toward High Capacity and Durable Potassium-Ion Battery Anodes. *Adv. Funct. Mater.* **2024**, *34*, 2409937. [CrossRef]
118. Yang, M.M.; Kong, Q.; Feng, W.; Yao, W. N/O double-doped biomass hard carbon material realizes fast and stable potassium ion storage. *Carbon* **2021**, *176*, 71–82. [CrossRef]
119. Kömür, A.I.; Kizil, Ç.; Karaman, C. Nature's blueprint for energy: Biomass-derived heteroatom-doped graphene materials for advanced energy applications. *Carbon Lett.* **2025**, *35*, 919–961. [CrossRef]
120. Cui, R.C.; Xu, B.; Dong, H.J.; Yang, C.C.; Jiang, Q. N/O Dual-Doped Environment-Friendly Hard Carbon as Advanced Anode for Potassium-Ion Batteries. *Adv. Sci.* **2020**, *7*, 1902547. [CrossRef]

121. He, B.; Feng, L.; Hong, G.; Yang, L.; Zhao, Q.; Yang, X.; Yin, S.; Meng, Y.; Xiao, D.; Wang, Y.; et al. A generic F-doped strategy for biomass hard carbon to achieve fast and stable kinetics in sodium/potassium-ion batteries. *Chem. Eng. J.* **2024**, *490*, 151636. [CrossRef]
122. Yu, J.; Kim, D.K.; Oh, H.G.; Park, S.K.; Yoo, Y. N, P co-doped 3D porous carbon with self-assembled morphological control via template-free method for potassium-ion battery anodes. *Rare Met.* **2024**, *43*, 4243–4252. [CrossRef]
123. Gong, J.; Zhao, G.; Feng, J.; An, Y.; Li, T.; Zhang, L.; Li, B.; Qian, Z. Controllable Phosphorylation Strategy for Free-Standing Phosphorus/Nitrogen Cofunctionalized Porous Carbon Monoliths as High-Performance Potassium Ion Battery Anodes. *ACS Nano* **2020**, *14*, 14057–14069. [CrossRef]
124. Chen, J.; Cheng, Y.; Zhang, Q.; Luo, C.; Li, H.Y.; Wu, Y.; Zhang, H.; Wang, X.; Liu, H.; He, X.; et al. Designing and Understanding the Superior Potassium Storage Performance of Nitrogen/Phosphorus Co-Doped Hollow Porous Bowl-Like Carbon Anodes. *Adv. Funct. Mater.* **2021**, *31*, 2007158. [CrossRef]
125. Dai, Y.; Qu, Z.T.; Wang, W.K.; Li, M.S.; Chen, K.X.; Lyu, S.S. Hollow carbon nanospheres with optimized nitrogen configuration controlled by heteroatom doping for high-performance potassium-ion storage. *Carbon* **2024**, *224*, 119051. [CrossRef]
126. Jin, S.; Liang, P.; Jiang, Y.; Min, H.; Niu, M.; Yang, H.; Zhang, R.; Yan, J.; Shen, X.; Wang, J. Preferentially engineering edge-nitrogen sites in porous hollow spheres for ultra-fast and reversible potassium storage. *Chem. Eng. J.* **2022**, *435*, 134821. [CrossRef]
127. Ao, X.; Kong, Y.; Zhao, S.; Chen, Z.; Li, Y.; Liao, X.; Tian, B. Metal-N Coordination in Lithium-Sulfur Batteries: Inhibiting Catalyst Passivation. *Angew. Chem. Int. Ed.* **2025**, *64*, e202415036. [CrossRef]
128. He, H.; Huang, D.; Tang, Y.; Wang, Q.; Ji, X.; Wang, H.; Guo, Z. Tuning nitrogen species in three-dimensional porous carbon via phosphorus doping for ultra-fast potassium storage. *Nano Energy* **2019**, *57*, 728–736. [CrossRef]
129. Yan, F.; Yang, Q.; Li, M.; Chen, G.; Zhang, W.; Chen, Y. Facile synthesis of hollow stalagmite-like N, S-doped C and its capacity attenuation mechanism as anodes in K-ion batteries. *Carbon* **2022**, *200*, 56–62. [CrossRef]
130. Cheng, G.; Zhang, W.; Wang, W.; Wang, H.; Wang, Y.; Shi, J.; Chen, J.; Liu, S.; Huang, M.; Mitlin, D. Sulfur and nitrogen codoped cyanoethyl cellulose-derived carbon with superior gravimetric and volumetric capacity for potassium ion storage. *Carbon Energy* **2022**, *4*, 986–1001. [CrossRef]
131. Kim, M.; Ma, L.; Li, Z.; Mai, W.; Amiralian, N.; Rowan, A.E.; Yamauchi, Y.; Qin, A.; Afzal, R.A.; Martin, D.; et al. N and S co-doped nanosheet-like porous carbon derived from sorghum biomass: Mechanical nanoarchitecturing for upgraded potassium ion batteries. *J. Mater. Chem. A* **2023**, *11*, 16626–16635. [CrossRef]
132. Jiao, R.; Deng, Z.; Lei, L.; Liu, Y.; Cui, J. S/N co-doped hierarchical porous carbon from lignite as high-performance anode for potassium-ion batteries. *J. Energy Storage* **2023**, *74*, 109486. [CrossRef]
133. Bi, K.; Wang, Y.; Zhou, G.Y. Hierarchical porous N/S-doped carbon with machine learning to predict advanced potassium-ion batteries. *J. Mater. Chem. A* **2023**, *11*, 11696–11703. [CrossRef]
134. Xu, D.; Cheng, Q.; Saha, P.; Hu, Y.; Chen, L.; Jiang, H.; Li, C. Engineering Se/N Co-Doped Hard CNTs with Localized Electron Configuration for Superior Potassium Storage. *Adv. Funct. Mater.* **2023**, *33*, 2211661. [CrossRef]
135. Lu, Y.; Liang, H.; Wang, X.; Zhang, H.; Shi, J.; Tian, W.; Chen, J.; Zhu, Y.; Huang, M.; Wang, H. Pearl-Necklace Structured Se-Doped Hollow Carbon Nanofibers for High-Capacity and Ultrastable Potassium Ion Storage. *Green Energy Environ.* 2025; *in press*. [CrossRef]
136. Jiang, Y.; Li, W.; Li, X.; Liao, Y.; Liu, X.; Yu, J.; Xia, S.; Li, W.; Zhao, B.; Zhang, J. Iodine-doped carbon nanotubes boosting the adsorption effect and conversion kinetics of lithium-sulfur batteries. *J. Colloid Interface Sci.* **2024**, *672*, 287–298. [CrossRef]
137. Zhang, Y.; Yang, Y.; Huang, C.; Fan, H.; Yuan, D.; Luo, W.B.; Hu, A.; Tang, Q.; Chen, X. Understanding the effect of I/N dual-doped hard carbon for high performance K-ion storage. *Electrochim. Acta* **2021**, *394*, 139146. [CrossRef]
138. Chen, H.; Wu, Y.; Xu, H.; Zhao, J.; Wang, J.; Ren, C.; Zhao, C.; Yang, R. Fluorine-doped carbon coating of $LiFe_{0.5}Mn_{0.5}PO_4$ enabling high-rate and long-lifespan cathode for lithium-ion batteries. *J. Power Sources* **2025**, *628*, 235892. [CrossRef]
139. Yang, L.; He, B.; Li, M.; Li, S.; Xiao, D.; Wang, Y.; Meng, Y.; Zhao, Q.; Yue, Q.; Feng, W. A fluorine/oxygen co-doping scheme for biomass carbon provides excellent rapid reaction kinetics for sodium/potassium-ion batteries. *Inorg. Chem. Front.* **2024**, *11*, 4672–4685. [CrossRef]
140. Chen, M.; Wang, W.; Liang, X.; Gong, S.; Liu, J.; Wang, Q.; Guo, S.; Yang, H. Sulfur/Oxygen Codoped Porous Hard Carbon Microspheres for High-Performance Potassium-Ion Batteries. *Adv. Energy Mater.* **2018**, *8*, 1800171. [CrossRef]
141. Fu, Y.; Shen, X.; You, J.; Yu, R.; Zheng, J.; Wu, B.; Soför, Z.; Wei, Q.; Yang, W. Extremely Durable K-Ion Batteries Enabled by Heteroatom Co-Doped Highly-Ordered Porous Carbon Spheres with Nearly 100% Capacity Retention up to 11,000 Cycles. *Nano Lett.* **2024**, *24*, 10759–10766. [CrossRef]
142. Lu, X.; Zhou, J.; Huang, L.; Peng, H.; Xu, J.; Liu, G.; Shi, C.; Sun, Z. Low-Temperature Carbonized N/O/S-Tri-Doped Hard Carbon for Fast and Stable K-Ions Storage. *Adv. Energy Mater.* **2024**, *14*, 2303081. [CrossRef]
143. Zhang, X.; Huang, R.; Wu, F.; Chen, R.; Li, L. Mixed-biomass engineering achieves multi-doped highly-disordered hierarchical flower-like hard carbon for advanced potassium-ion battery. *Nano Energy* **2023**, *117*, 108913. [CrossRef]

144. Wang, R.; Feng, Y.; Li, D.; Li, K.; Yan, Y. Towards the sustainable production of biomass-derived materials with smart functionality: A tutorial review. *Green Chem.* **2024**, *26*, 9075–9103. [CrossRef]
145. Yang, M.M.; Kong, Q.; Feng, W.; Yao, W.; Wang, Q. Hierarchical porous nitrogen, oxygen, and phosphorus ternary doped hollow biomass carbon spheres for high-speed and long-life potassium storage. *Carbon Energy* **2022**, *4*, 45–59. [CrossRef]
146. Hu, P.; Xiao, F.; Wu, Y.; Yang, X.; Li, N.; Wang, H.; Jia, J. Covalent encapsulation of sulfur in a graphene/N-doped carbon host for enhanced sodium-sulfur batteries. *Chem. Eng. J.* **2022**, *443*, 136257. [CrossRef]
147. Zhao, Q.; Zheng, Q.; Li, S.; He, B.; Wu, X.; Wang, Y.; Wang, Q.; Meng, Y.; Xiao, D. Nitrogen/oxygen/sulfur tri-doped hard carbon nanospheres derived from waste tires with high sodium and potassium anodic performances. *Inorg. Chem. Front.* **2023**, *10*, 2574–2585. [CrossRef]
148. Liu, Y.; Dai, H.; An, Y.; Fu, L.; An, Q.; Wu, Y. Facile and scalable synthesis of a sulfur, selenium and nitrogen co-doped hard carbon anode for high performance Na- and K-ion batteries. *J. Mater. Chem. A* **2020**, *8*, 14993–15001. [CrossRef]
149. Gong, J.; Zhao, G.; Feng, J.; Wang, G.; Shi, Z.; An, Y.; Zhang, L.; Li, B. Control of the structure and composition of nitrogen-doped carbon nanofoams derived from CO_2 foamed polyacrylonitrile as anodes for high-performance potassium-ion batteries. *Electrochim. Acta* **2021**, *388*, 138630. [CrossRef]
150. Yang, H.; Lei, L.; Zhao, Y.; Lan, D.; An, S.; Liu, Y.; Cui, J. Lignite-based hard carbon for high-performance potassium-ion battery anode. *Ionics* **2024**, *30*, 3253–3263. [CrossRef]
151. Xie, X.; Qi, S.; Wu, D.; Wang, H.; Li, F.; Peng, X.; Cai, J.; Liang, J.; Ma, J. Porous surfur-doped hard carbon for excellent potassium storage. *Chin. Chem. Lett.* **2020**, *31*, 223–226. [CrossRef]
152. Nan, D.; Wu, Z.; Lu, Z.; Qin, L.; Zhang, B.; Chen, L.; Zhang, D.; Xu, S. Facile preparation of heteroatom S doped dumbbell-like hard carbon for boosting potassium-ion storage capability. *Electrochim. Acta* **2023**, *465*, 143019. [CrossRef]
153. Zhang, Y.; Li, L.; Xiang, Y.; Zou, G.; Hou, H.; Deng, W.; Ji, X. High Sulfur-Doped Hard Carbon with Advanced Potassium Storage Capacity via a Molten Salt Method. *ACS Appl. Mater. Interfaces* **2020**, *12*, 30431–30437. [CrossRef]
154. Zhang, K.; He, Q.; Xiong, F.; Zhou, J.; Zhao, Y.; Mai, L.; Zhang, L. Active sites enriched hard carbon porous nanobelts for stable and high-capacity potassium-ion storage. *Nano Energy* **2020**, *77*, 105018. [CrossRef]
155. Chong, S.; Yuan, L.; Li, T.; Shu, C.; Qiao, S.; Dong, S.; Liu, Z.; Yang, J.; Liu, H.K.; Dou, S.X.; et al. Nitrogen and Oxygen Co-Doped Porous Hard Carbon Nanospheres with Core-Shell Architecture as Anode Materials for Superior Potassium-Ion Storage. *Small* **2022**, *18*, 2104296. [CrossRef]
156. Tao, S.; Xu, W.; Zheng, J.; Kong, F.; Cui, P.; Wu, D.; Qian, B.; Chen, S.; Song, L. Soybean roots-derived N, P Co-doped mesoporous hard carbon for boosting sodium and potassium-ion batteries. *Carbon* **2021**, *178*, 233–242. [CrossRef]
157. Wang, Q.; Wang, Y.; Zeng, J.; Xu, C.; Liu, P.; Meng, Y.; Zhang, C.; Wang, Y.; Gao, L.; Ding, R.; et al. Nitrogen and phosphorus co-doped carbon for improving capacity and rate performances of potassium ion batteries. *Flatchem* **2022**, *34*, 100398. [CrossRef]
158. Liu, Y.; Dai, H.; Wu, L.; Zhou, W.; He, L.; Wang, W.; Yan, W.; Huang, Q.; Fu, L.; Wu, Y. A Large Scalable and Low-Cost Sulfur/Nitrogen Dual-Doped Hard Carbon as the Negative Electrode Material for High-Performance Potassium-Ion Batteries. *Adv. Energy Mater.* **2019**, *9*, 1901379. [CrossRef]
159. Wang, L.; Li, S.; Li, J.; Yan, S.; Zhang, X.; Wei, D.; Xing, Z.; Zhuang, Q.; Ju, Z. Nitrogen/sulphur co-doped porous carbon derived from wasted wet wipes as promising anode material for high performance capacitive potassium-ion storage. *Mater. Today Energy* **2019**, *13*, 195–204. [CrossRef]
160. Li, W.; Wang, D.; Gong, Z.; Guo, X.; Liu, J.; Zhang, Z.; Li, G. Superior potassium-ion storage properties by engineering pseudocapacitive sulfur/nitrogen-containing species within three-dimensional flower-like hard carbon architectures. *Carbon* **2020**, *161*, 97–107. [CrossRef]

Disclaimer/Publisher's Note: The statements, opinions and data contained in all publications are solely those of the individual author(s) and contributor(s) and not of MDPI and/or the editor(s). MDPI and/or the editor(s) disclaim responsibility for any injury to people or property resulting from any ideas, methods, instructions or products referred to in the content.